High Speed Multiple-Pass Cavity Scanning Optical Delay Line for Real-Time High Resolution Optical Coherence Tomography (OCT)

Zhijun Zhao

A thesis

in

The department

of

Electrical and Computer Engineering

Presented in Partial Fulfillment of the Requirements

for the Degree of Master of Applied Science (Electrical and Computer Engineering) at

Concordia University

Montreal, Quebec, Canada

December 2005

Your file Votre référence
ISBN: 0-494-14291-X
Our file Notre référence
ISBN: 0-494-14291-X

Abstract

High speed multiple-pass cavity scanning optical delay line
for real-time high resolution optical coherence tomography (OCT)

Zhijun Zhao

Firstly, the basic theory of the optical coherence tomography (OCT) is reviewed. Optical delay line is one of important parts in OCT. Several types of optical delay lines which were proposed and demonstrated are briefly described including their advantages and disadvantages.

In this work, a novel multiple-pass cavity optical delay line (MPC-ODL) is proposed and analyzed. The proposed delay line consists of four mirrors, one lens and one resonant scanner. In this proposed delay line, the path delay is obtained by scanning a tilting mirror and magnified by the multiple-pass optical cavity. Thus, for a small scanning angle, a large path delay can be obtained. This delay line is especially suitable for the OCT system that will generate the large dimension images at video rate with high resolution. However, due to multiple-pass cavity used in the proposed delay line, false interference signal may be created besides OCT signal. In order to reduce the false interference signal generation, some crucial parameters of the proposed delay line have to be carefully chosen. Principle of how to choose the optical component parameters is given.

The proposed delay line combined with OCT is verified by computer simulation. Characterization of the delay line is done by simulation and it is shown that the scanning repetition rate of 16 kHz, the total path delay of 3 mm, and the scan velocity of 71.3 m/s can be achieved. The proposed delay line can support OCT system with dynamic range over 110 dB.

The proposed delay line can support a further higher scanning repetition rate, such as 32kHz.

Acknowledgements

I wish to express my most sincere appreciation to my supervisor Dr. John Zhang for his help and support during my study in Concordia University. His insight, expertise and wealth of knowledge are invaluable to me. Without his help, I could not finish this study.

I would like to thanks Shuang Jin for the simulation discussion from which I broadened my vision and consolidated my understanding of my research subject.

Finally, I would like to thank my family, especially my wife Wenrui, for all the love and support from them.

Contents

List of figures

List of tables

Chapter 1 Introduction

1.1 Motivation

Optical coherence tomography (OCT) is a noninvasive imaging technique which provides microscopic tomography of biological tissues [1]. Basically, OCT is preferred to have a high axial resolution, and to generate the images at real-time video rate (30 frames per second). Axial resolution in OCT is inversely proportional to optical source bandwidth. Axial resolution of 1-3 μm was demonstrated by use of state-of-the-art low coherence light sources [2-4]. A high speed scanning optical delay line (SODL) in the reference arm of the OCT system is required to acquire images, preferably with real-time video rate. An OCT image (B-scan) is built up as a series of consecutive axial depth scans (A-scans). A-scan images must be collected at a rate equal to the frame rate multiplying the numbers of A-scans per frame. In order to image at video rate with 250 transverse lines (A-scans) per frame, 7500 A-scans per second are required. To date, the commonly used SODL in OCT systems is Fourier-domain optical delay line (FD-ODL) based on a diffraction grating and tilted mirror [5-7]. In this kind of FD-ODL, the incident broadband light is diffracted by the grating and spectrally dispersed, a large-size scanning mirror is required to accommodate those optical spectral components. The dimension of the scanning mirror in the high resolution FD-ODL limits the scanning speed of below 4 kHz. Another FD-ODL based on grating and polygonal scanner was demonstrated at 4 kHz with very good linearity, but duty cycles are limited [8]. Alternatively, some time-domain optical delay lines (TD-ODL) were proposed and demonstrated at several kHz repetition rate [9, 10]. Recently, an all-reflective delay line was demonstrated in order to remove dispersion effect of the delay line in OCT [11]. It was shown that a scanning repetition rate of 4.1 kHz was achieved and is limited by the maximum scanning mirror size. Currently, optical scanner repetition frequencies of 4, 6, and 8 kHz can be obtained with the scanning mirror size of 8, 7, and 5 mm, respectively. A high resolution video

rate OCT images are preferred to have at least 500 transverse lines, which requires an optical delay line with 15 kHz repetition frequency.

Therefore the current FD-ODL and TD-ODL are not fully satisfied for the high resolution video rate OCT systems. There is a good motivation to investigate a high speed delay line for the high resolution video rate OCT systems.

1.2 Organization of the thesis

Chapter 1 is an introduction and background section. The basic theory of the OCT system is presented. A detailed review of the optical delay line is also presented in this section.

In Chapter 2, a novel high speed delay line is proposed and the theoretical analysis is presented. Some parameters, which are crucial to the proposed delay line, are analyzed in detail in Section 2.2. The principle of components selection is given in Section 2.3.

In Chapter 3, some computer simulations are done to verify the theory of the proposed delay line.

Chapter 4 is a conclusion section.

The goal of following sections is to review the basic concept of optical coherence tomography technique. Section 1.4 will review the field of scanning optical delay lines (SODLs), emphasizing devices that have been applied in OCT imaging.

1.3 Introduction of OCT

In optical coherence tomography, the principles of interferometry with low temporal coherence light and optical heterodyne detection are combined to obtain both a high axial resolution (1 – 10 μm) and a high sensitivity (more than 100 dB) to light that is weakly reflected from the sample being imaged. One, two, and three dimensional images of the internal microstructure of a

sample's optical properties such as refractive index, absorption coefficient, and scattering coefficient can be obtained.

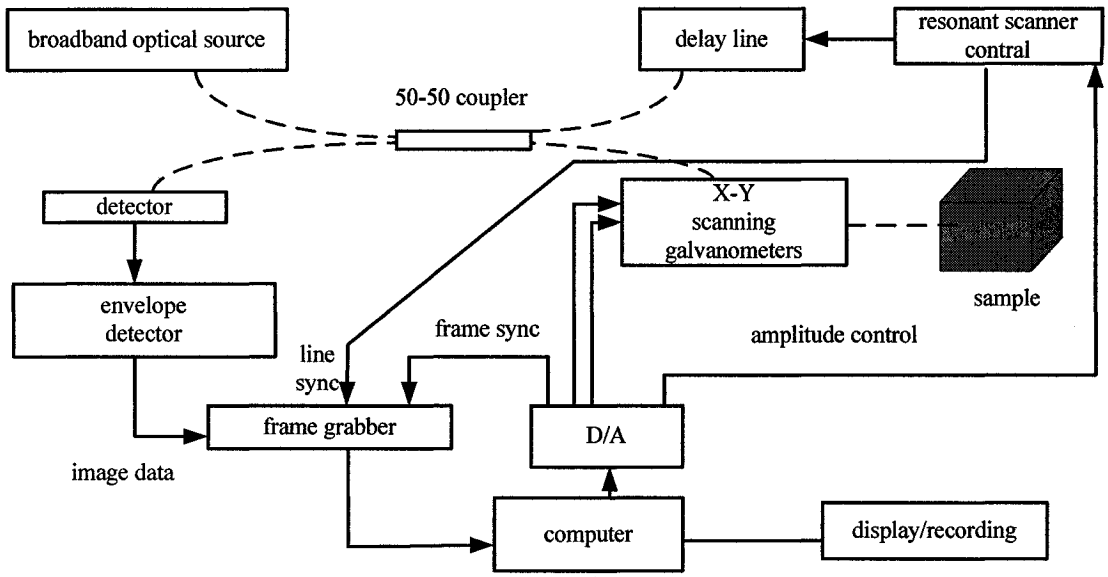

Figure 1-1. Schematic of the high speed OCT system. The broken lines represent optical paths and the solid black lines represent electronic paths [7].

The schematic of the OCT system is shown in Figure 1-1. Low coherence light is coupled into a fiber coupler, which is served as an interferometer, and divided into reference and sample paths. Light retroreflected from a scanning reference mirror is recombined in the coupler with light backscattered form the sample under interrogation. Time-of-flight information is obtained in the interference signal between the reference and sample beams, which is detected by a photodiode followed by signal processing electronics and computer data acquisition [7].

1.3.1 Low coherence interferometry and axial resolution

The basic principle of the OCT is given in following sections.

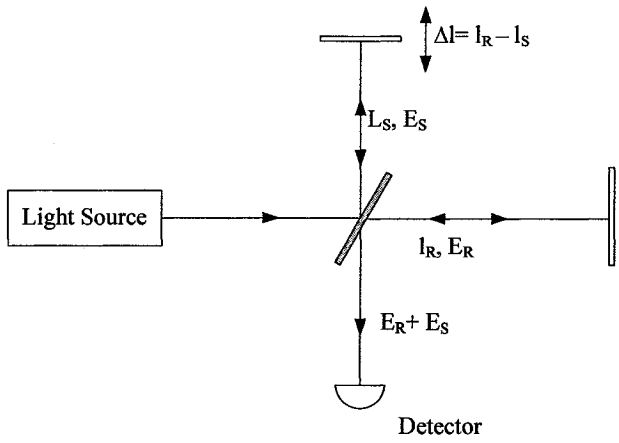

Figure 1-2. The Michelson interferometer

1.3.1.1 Interferometer with coherent light

Consider the simplified schematic of the Michelson interferometer shown in Figure 1-2, where sample has been replaced by a perfectly reflecting mirror. Light from the source is divided at a beam-splitter into reference and sample beams. Light reflected from the reference and sample mirrors is recombined at the same beam-splitter and incident on a detector. The reference and sample mirrors are positioned at distances l_R and l_S, respectively, from the beam-splitter. If the light source is perfectly coherent (i.e., monochromatic), then reflection from the reference and sample mirrors produces a sum of two monochromatic electric field components E_R and E_S at the detector. These fields may be expressed by [13]

$$E_R = A_R \exp[-j(2\beta_R l_R - \omega t)] \text{ and } E_S = A_S \exp[-j(2\beta_S l_S - \omega t)] \quad \text{Eq. 1-1}$$

where ω is the optical frequency of the light source and β is the propagation constant. The factor of 2 multiplying the propagation constants β_R and β_S arise from the round-trip propagation of light to and from the reference and sample mirrors.

In general, the time-averaged photocurrent I of the detector is given by [13]

$$I = \left\langle \frac{\eta e}{h\nu}\left(\frac{|E_R + E_S|^2}{2\eta_0} \right) \right\rangle \quad \text{Eq. 1-2}$$

where η is the detector quantum efficiency, e is the electronic charge, $h\nu$ is the photon energy, and η_0 is the intrinsic impedance of free space. For monochromatic fields, Eq. 1-2 can be written

$$I = \frac{\eta e}{h\nu}\left(\frac{1}{\eta_0} \right)\left[\frac{1}{2}|A_R|^2 + \frac{1}{2}|A_S|^2 + real\{E_R E_S^*\} \right] \quad \text{Eq. 1-3}$$

where the term

$$real\{E_R E_S^*\} = A_R A_S \cos(2\beta_R l_R - 2\beta_S l_S) \quad \text{Eq. 1-4}$$

describes the variation of the photocurrent with the positions of the reference and sample mirrors. In free space, the propagation constants are equal for the reference and sample fields, giving $\beta_R = \beta_S = 2\pi/\lambda$ and

$$real\{E_R E_S^*\} = A_R A_S \cos\left(2\pi \frac{\Delta l}{\lambda/2} \right) \quad \text{Eq. 1-5}$$

where $\Delta l = l_R - l_S$ is the mismatch in distance between the reference and sample beam paths [13].

1.3.1.2 Interferometer with low coherence light

A low coherence light source consists of a finite bandwidth of frequencies rather than just a single frequency. The analysis above can be extended to account for partially coherent light by integrating the cross-spectral term $E_R E_S^*$ over the harmonic content of the light source. We allow the reference and sample fields to be functions of frequency [13]

$$E_R = A_R(\omega)\exp\{-j[2\beta_R(\omega)l_R - \omega t]\} \quad \text{Eq. 1-6}$$

$$E_S = A_S(\omega)\exp\{-j[2\beta_S(\omega)l_S - \omega t]\} \quad \text{Eq. 1-7}$$

The interference signal at the photo-detector is proportion to the sum of the interference due to each monochromatic plane wave component, according to [13]

$$I \propto real\left\{\int_{-\infty}^{\infty} E_S(\omega)E_R(\omega)^* \frac{d\omega}{2\pi}\right\} = real\left\{\int_{-\infty}^{\infty} S(\omega)\exp[-j\Delta\Phi(\omega)]\frac{d\omega}{2\pi}\right\} \quad \text{Eq. 1-8}$$

where we have used the definitions [13]

$$S(\omega) = A_S(\omega)A_R(\omega)^* \quad \text{Eq. 1-9}$$

and

$$\Delta\Phi(\omega) = 2\beta_R(\omega)l_R - 2\beta_S(\omega)l_S \quad \text{Eq. 1-10}$$

If the sample and reference arm fields have the same spectral components as the light source (i.e., if the reflectors in each arm and fiber beam-splitter are spectrally uniform), then $S(\omega)$ essentially equivalent to the power spectrum of the light source. $\Delta\Phi(\omega)$ expresses the phase mismatch at the detector of each frequency component [13].

1.3.1.3 Nondispersive Medium

Consider the case where the sample and reference arms consist of a uniform, linear, nondispersive medium. Let the spectrum of the light source $S(\omega-\omega_0)$ be band limited with a center frequency of ω_0. We assume that the propagation constants β in each arm are the same and rewrite them as first-order Taylor expansions around the center frequency

$$\beta_S(\omega) = \beta_R(\omega) = \beta(\omega_0) + \beta'(\omega_0)(\omega-\omega_0) \quad \text{Eq. 1-11}$$

Then the phase mismatch $\Delta\Phi(\omega)$ is determined solely by the length mismatch $\Delta l = l_R - l_S$ between the reference and sample arms through [13]

$$\Delta\Phi(\omega) = \beta(\omega_0)(2\Delta l) + \beta'(\omega_0)(\omega-\omega_0)(2\Delta l) \quad \text{Eq. 1-12}$$

The integral over the power spectral density in Eq. 1-8 becomes

$$I \propto real\left\{\exp(-j\omega_0\Delta\tau_p)\int_{-\infty}^{\infty} S(\omega-\omega_0)\exp[-j(\omega-\omega_0)\Delta\tau_g]\frac{d(\omega-\omega_0)}{2\pi}\right\} \quad \text{Eq. 1-13}$$

where the phase delay mismatch $\Delta\tau_p$ and the group delay mismatch $\Delta\tau_g$ are defined as [13]

$$\Delta\tau_p = \frac{\beta(\omega_0)}{\omega_0}(2\Delta l) = \frac{2\Delta l}{v_p} \qquad \text{Eq. 1-14}$$

And

$$\Delta\tau_g = \beta'(\omega_0)(2\Delta l) = \frac{2\Delta l}{v_g} \qquad \text{Eq. 1-15}$$

Thus, $v_p = \omega_0 / \beta(\omega_0)$ corresponds to the center frequency phase velocity and $v_g = 1/\beta'(\omega_0)$ is the group velocity [13].

1.3.1.4 Gaussian power spectrum and nondispersive medium.

We assume that the light source has a Gaussian power spectral density given by

$$S(\omega - \omega_0) = \left(\frac{2\pi}{\sigma_\omega^2}\right)^{\frac{1}{2}} \exp\left[-\frac{(\omega-\omega_0)^2}{2\sigma_\omega^2}\right] \qquad \text{Eq. 1-16}$$

which has been normalized to unit power

$$\int_{-\infty}^{\infty} S(\omega)\frac{d\omega}{2\pi} = 1 \qquad \text{Eq. 1-17}$$

and where ω_0 is defined as the central frequency and $2\sigma_\omega^2$ is the standard deviation power spectral bandwidth (radians per second). Therefore the interferometric photocurrent is given by [13]

$$I \propto \exp\left(-\frac{\Delta\tau_g^2}{2\sigma_\tau^2}\right)\exp(-j\omega_0\Delta\tau_p) \qquad \text{Eq. 1-18}$$

where the real{} notation has been discarded for convenience. Eq. 1-18 shows that the interferometric term of the photocurrent consists of a carrier and an envelope. The envelop, which determines the axial point spread function of the interferometer, is essentially the inverse Fourier transform of the source power spectrum $S(\omega - \omega_0)$. The photocurrent contains a Gaussian envelop with a characteristic standard deviation temporal width $2\sigma_\tau$ (seconds) that is inversely proportional to the power spectral bandwidth [13]

$$2\sigma_\tau = \frac{2}{\sigma_\omega} \qquad \text{Eq. 1-19}$$

Note that $\sigma_\tau \sigma_\omega = 1$ (i.e., the time-frequency uncertainty relation is minimized for a Gaussian waveform). The envelop falls off quickly with increasing group delay mismatch $\Delta\tau_g$ and is modulated by interference fringes that oscillate with increasing phase delay mismatch $\Delta\tau_p$. Thus, Eq. 1-8 defines the axial resolving properties of the OCT system. The detector sees interference fringes only when the reference and sample arm lengths are matched, so the group delay mismatch falls within the Gaussian envelop:

$$-\sigma_\tau < \beta'(\omega_0)(2\Delta l) < \sigma_\tau \qquad \text{Eq. 1-20}$$

The standard deviation axial resolution, or width if the axial point spread function (i.e., the $\pm\sigma_\tau$ width of the Gaussian envelope in units of the length mismatch Δl) is:

$$\Delta l_{SD} = \frac{1}{\beta'(\omega_0)\sigma_\omega} = \frac{v_g}{\sigma_\omega} \qquad \text{Eq. 1-21}$$

For propagation in free space, both the phase velocity and group velocity equal the speed of light c, therefore,

$$\Delta l_{SD} = \frac{c}{\sigma_\omega} \qquad \text{Eq. 1-22}$$

showing that the axial resolution is inversely proportional to the bandwidth [13].

For a Gaussian with standard deviation σ, the FWHM equal $2\sigma\sqrt{2\ln 2}$. Thus, for the interferometer in free space, the FWHM resolution Δl_{FWHM} is related to the FWHM wavelength bandwidth $\Delta\lambda$ for a Gaussian source by

$$\Delta l_{FWHM} = \frac{2\ln 2}{\pi}\left(\frac{\lambda_0^2}{\Delta\lambda}\right) \qquad \text{Eq. 1-23}$$

where λ_0 is the center wavelength [13].

1.3.2 Signal-to-noise ratio (SNR) of OCT system

In Oct as in any optical heterodyne detector, the detected signal-to-noise ratio (SNR) in the shot noise limit is proportional to the optical power illuminating the sample and inversely proportional to the detection bandwidth [14].

$$SNR = \frac{\rho P_s R_s}{2eB} \qquad \text{Eq. 1-24}$$

where P_s is the power incident on the sample, R_s is the power reflectivity of the power, e is the electronic charge, B is the detector bandwidth, and ρ is the detector responsivity. In OCT the detected signal bandwidth Δf is proportional to the image acquisition rate [15]. Therefore, an increase in image acquisition rate will increase the signal bandwidth. In order to maintain SNR while detecting the entire signal bandwidth, any increase in image acquisition rate must be accompanied by a proportional increase in source optical power.

When the pathlength difference is scanned by a scanning delay line in the reference arm, the photodetector response is a time domain signal related to the interferometric autocorrelation by the scan velocity of the delay. The carrier of the detector response signal is related to the carrier of the autocorrelation by the phase delay scan speed, and hence the center frequency Δf can be written in terms of the center of the optical source spectrum [7]:

$$f_0 = \frac{V_\Phi k_0}{2\pi} = v_0 \frac{V_\Phi}{c} = \frac{V_\Phi}{\lambda_0} \qquad \text{Eq. 1-25}$$

where V_Φ is the scan speed of the phase delay, v_0 and λ_0 are the center frequency and the center wavelength, respectively, of the optical source. The carrier frequency corresponds to the Doppler shift frequency of the center wavelength component of the reference arm light, and equivalently to the beat frequency of the optical heterodyne detector response. The frequency components of the detector response signal, expressed as offset from the carrier frequency $f' = (f - f_0)$, are related to the complex envelope of the autocorrelation by the scan speed of the group delay. They

can thus be written in terms of the offset frequency $v' = (v - v_0)$, or wavelength components of the optical source [7]

$$f' = v' \frac{V_g}{c} = \left(\frac{1}{\lambda} - \frac{1}{\lambda_0} \right) V_g \qquad \text{Eq. 1-26}$$

or

$$\Delta f = \Delta v \frac{V_g}{c} = \frac{\Delta \lambda}{\lambda_0^2} V_g \qquad \text{Eq. 1-27}$$

where V_g is the scan speed of the group delay. The autocorrelation function corresponds to the point spread function of the OCT system in the axial direction [16]. In designing a practical OCT system, therefore, the full information bandwidth of the signal must be detected in order to maximize spatial resolution. It is desired, however, to reject frequencies outside of the information bandwidth in order to maximize system SNR. Assuming a Gaussian optical source spectrum (and therefore a Gaussian autocorrelation function), the ideal detector bandwidth corresponds to approximately two times the signal bandwidth [14]. Therefore the SNR of OCT in the shot noise limit, using the ideal detection bandwidth, becomes [7]:

$$SNR = \frac{\rho P_s R_s \lambda_0^2}{4e \Delta \lambda V_g} \qquad \text{Eq. 1-28}$$

Thus, it can be seen that if the bandwidth of the interferometric signal is increased by rapidly scanning the group delay, the source power must be proportionally increased in order to maintain the SNR [7].

1.4 Optical delay lines

This section will review the field of scanning optical delay lines (SODLs).

In OCT technique, the optical delay line is the main element of the reference arm. The interference signal occurs when the optical pathlength in the sample arm of the interferometer coincides with that in the reference arm. The length of the reference arm is scanned periodically .

The working pathlength scanning range, pathlength scan velocity, linearity, duty cycle, and repetition rate are the major parameters of SODL [13].

The working pathlength scanning range (in meters per scan) is the portion of the delay sweep during which measurement can be made. In other words, this parameter refers to the depth range that will be imaged by the OCT system. It is important to note that group delay (as opposed to phase delay) sets the location of the coherence gate in OCT; therefore, this parameter specifically refers to the working scan range of the group delay. The desired range depends on the application and is determined by the scale of the features to be imaged and tissue attenuation [13].

The scan velocity (m/s) of the phase delay V_p determines the Doppler shift of the reference light and therefore the center frequency of the detected signal. The scan velocity of the group delay V_g, determines the bandwidth of the detected signal and relates to the imaging sweep. This parameter also goes to the fundamental trade-off between imaging speed and sensitivity in OCT.[13].

The scan repetition rate (in scans per second or Hertz) is the number of pathlength scans performed every second, or the inverse of the total scan period. This parameter depends on the scan length and scan velocity. and it is important for determining the image frame rate (images per second) of the OCT system [13].

The pathlength scan duty cycle is defined as the usable fraction of the total scan period. This parameter can be calculated from the preceding three parameters [13]

In many applications it is desirable to have simultaneously a high repetition rate, large scanning amplitude and high duty cycle to improve Signal-to-Noise Ratio (SNR) [14]. In designing a reference arm delay line, one must also consider parameters such as the scan depth determined by the maximum group delay, the linearity of the group delay in order to minimize the distortion of the images, the cost and availability of components and a modulation compatible with available data-acquisition hardware [13].

The scanning optical delay lines (ODLs) that will be reviewed here can be loosely classified into five main categories [13]:

1. ODLs that are based on linear translation of retroreflective elements
2. ODLs that vary optical pathlength by rotational methods
3. ODLs that are optical fiber stretches
4. ODLs that are based on group delay generation using Fourier domain optical pulse shaping technology
5. Optical frequency comb generators

1.4.1 SODLs based on linear translation of retroreflective elements

1.4.1.1 Linear Translator Mounted Retroreflector

The simplest SODL is a retroreflector mounted on a linear translating stage. The reference light is collimated and directed toward the retroreflector, which redirects the light back to the collimator, which re-couples the light into the delivery fiber. The retroreflector is mounted on a linear translating stage in order to scan the delay [13].

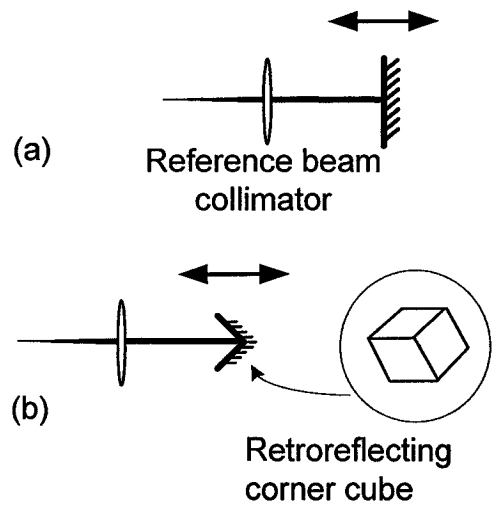

Figure 1-3. Schematic of an optical delay line consisting of a fixed delivery fiber and collimating lens plus a retroreflector mounted on a linear translating stage. A flat mirror (a) or a corner-cube retroreflector (b) can be used as the retroreflecting element [13].

A primitive delay line is a mechanically translating mirror, which is driven by a linear motor, or a piezoelectric transducer. It is the most obvious example of a delay line.

1.4.1.2 Multipass Translating Retroreflector

The scan range and velocity of a translating retroreflector can be amplified by allowing the reference light to make multiple passes. In other words; if the reference light reflects twice off a mirror moving at a scan velocity s, then the effective scan velocity (also called scan speed) is 2s [13].

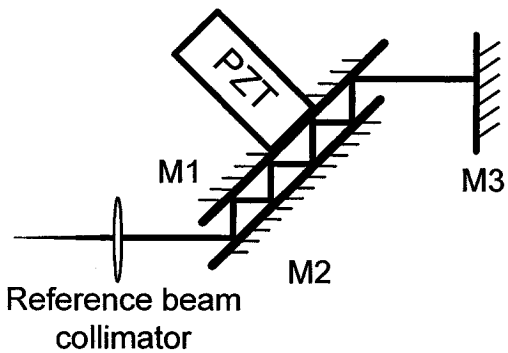

Figure 1-4. Schematic of an optical delay line consisting of a fixed delivery fiber, collimating lens, a parallel pair of mirrors and a retroreflecting mirror. One of the parallel mirrors is translated with a piezoelectric transducer [13].

1.4.1.3 Galvanometer-Mounted Retroreflector

An alternative to a linear stage actuator is a galvanometric scanner. Although the galvanometer is a rotational actuator, approximately linear translation can be effected by mounting a corner-cube retroreflector on a swing arm that is mounted on the galvanometer shaft. A corner-cube retroreflector is used to ensure that the light is retroreflected independently of the angle of the swing arm. In many respects, this SODL is very similar to the linear stage mounted retroreflector, but this configuration is capable of higher scan velocities and therefore higher scan repetition rates [13].

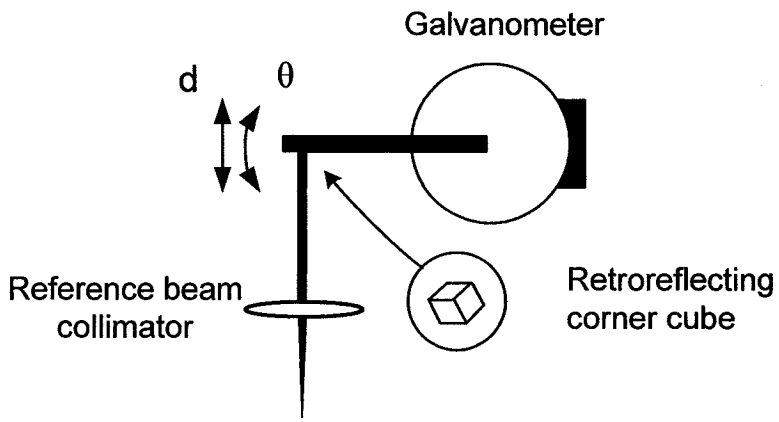

Figure 1-5. Schematic of an optical delay line consisting of a fixed delivery fiber and collimating lens and a corner-cube retroreflector mounted on a swing arm mounted on a galvanometer scanner [13].

1.4.1.4 High-speed path scanning with a multiple-pass cavity delay line.

A simple and low-cost scan was described which uses a multipass cavity to generate large group delays by translating one of the cavity mirrors slightly. The delay line uses a multipass mirror geometry that accumulates differential delays with each pass, enabling millimeter delays to be generated with tens of micrometer mirror displacements. The minimum required mirror displacement to achieve millimeters of path length scanning can thus be reduced when the number of bounces is increased on the cavity mirrors [10].

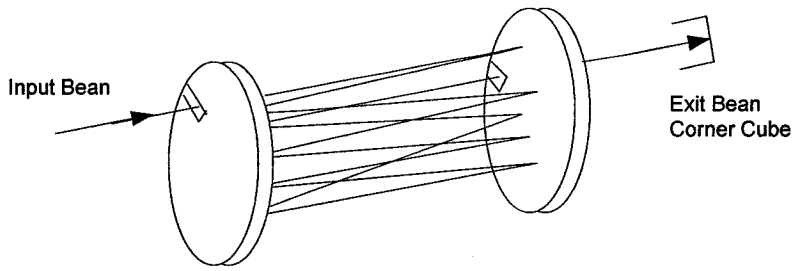

Figure 1-6. Schematic of the multipass cavity, which is formed by use of two symmetric broadband gold mirrors [10].

1.4.2 SODLs with varying optical pathlength by rotational methods

It is advantageous to use rotational motion-based devices instead of vibrating devices to generate optical path-length scanning. Once a steady rotation speed has been reached, a small amount of energy is required for maintaining rotation speed. This kind of delay line converts a small-angle rotation into a longitudinal optical path-length change [13].

1.4.2.1 Rotating cube

The optical pathlength (OPL) that a beam traverses can be scanned rapidly by passing the beam through a glass cube rotating at a constant speed. As the glass cube rotates, the thickness of glass that the beam passes through changes, and therefore the OPL changes [5].

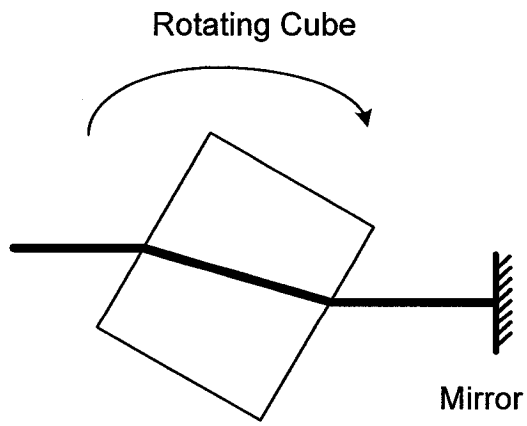

Figure 1-7. Rotating cube that operates with single pass, no internal reflections [13].

A cube can be rotated rapidly, generating delay sweeps at repetition rates much higher than those of the SODLs described so far. Several configurations based on this principle have been implemented. The pathlength scan range depends on the size of the cube as well as the configuration i.e. (how many passes through the cube).

The pathlength scan range is easily adequate for OCT, even with a small cube, but the scan range is not adjustable. It is fixed for a given cube size. The scan velocity depends on the configuration, the cube size and the cube rotation speed [13].

1.4.2.2 Scanning mirror

As with the rotating cubes and the galvanometer-mounted retroreflector, the motivation for using a rotational scanning element is speed. In addition to an angular scanning mirror, three additional mirrors and a lens are used. This configuration reflects the beam four times off the scanning mirror, amplifying the scan length and velocity by 4. All of the pathlength variation arises from the pivot of scanning mirror, so that there is an axial shift imposed on the beam in addition to the angular scan. In other words, if the beam were reflected from the pivot of scanning mirror, then no pathlength variation would result from scanning the mirror [9].

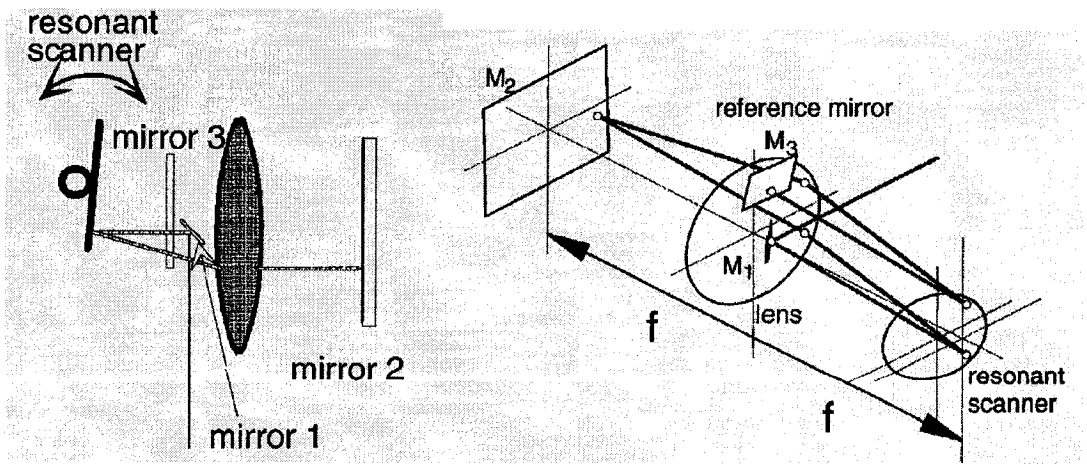

Figure 1-8. Schematic illustrations of an SODL. Here pathlength variation is made by transformation of an angular mirror scan to pathlength variation [9].

1.4.2.3 Rotary mirror array for high-speed optical coherence tomography

This is a novel design for implementing a periodic modulation of the optical path length in the reference arm, which consist of a DC modulator, a mirror array with internal reflections, and a convex lens [17].

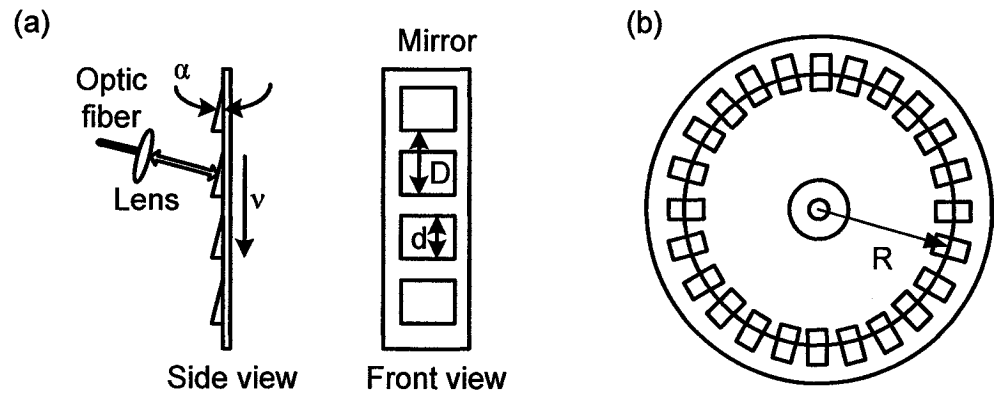

Figure 1-9. (a) Optical delay line with a section of an infinite linear mirror array. (b) Rotary mirror array derived from the linear array [17].

The principle of this delay line is quite simple. Mirrors are deployed uniformly on a planar base. Their reflected facets are tilted at a small angle with respect to the base. The optics of the reference arm is arranged so that the reference beam hits a mirror surface perpendicularly and is reflected back along the same path into the optical fiber. When the mirror array moves at a constant speed, the optical path length will be modulated periodically. Within each period, the change of optical path length is a linear function of time [17].

1.4.2.4 Kilohertz SODL employing a prism array.

It has been reported a Kilohertz SODL employing a set of identical wedge prism. The wedge prism are aligned with one another and uniformly disposed on a rotational wheel. The optical path length of a light beam is scanned as the prism pass through the beam periodically. Figure 1-10

illustrates a first embodiment of the Kilohertz SODL. The Kilohertz SODL consist of a prism array mounted evenly on a rotational wheel, a stationary prism, and a retroreflector. All prisms are identical. Each prism has a right angle and a wedge angle [18].

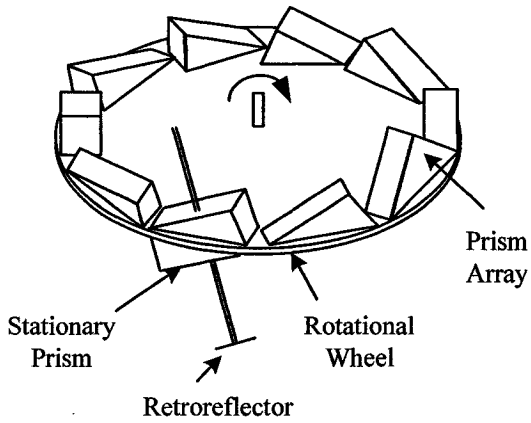

Figure 1-10. First embodiment of the kilohertz SODL employing a prism array mounted on a rotational wheel. The prism array is mounted in a complementary orientation with a stationary prism [18].

The prism array is mounted along a perimeter of the rotational wheel. The inclined surface of each prism is mounted parallel to the flat surface of the wheel. The stationary prism and the prism array are arranged in a complementary orientation. A light beam incident close to the normal of the second surface of the stationary prism remains substantially in the same direction as it passes through the stationary prism and any prism of the array. As the wheel rotates, the prisms of the array move across the light beam consecutively. The amount of glass through which the light beam passes is substantially as a sawtooth function of time [18].

A second embodiment of the Kilohertz SODL is illustrated in Figure 1-11. The achievable specifications or the second embodiment are similar to those of the first one [18].

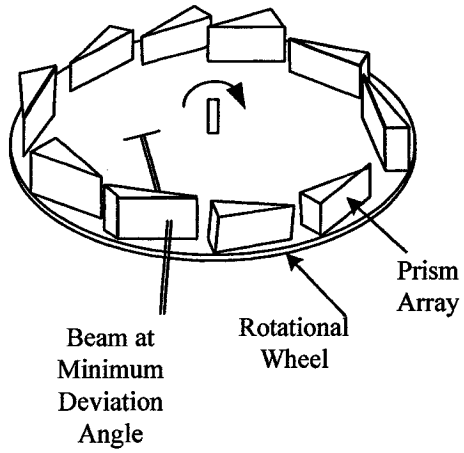

Figure 1-11. Second embodiment of the Kilohertz SODL employing a prism array mounted on a rotational wheel. The prism array is mounted to enable the use of minimum deviation angle [18].

1.4.2.5 All-reflection delay line with scanning mirror

Recently a rapid-scanning all-reflective optical delay line (RSAD) is reported. This RSAD consists of three mirrors (shown in Figure 1-12): one flat mirror driven by a resonant scanner to scan a collimated bean, one curved mirror to focus the collimated bean, and one flat mirror to retroreflect the focused bean back to the system [11].

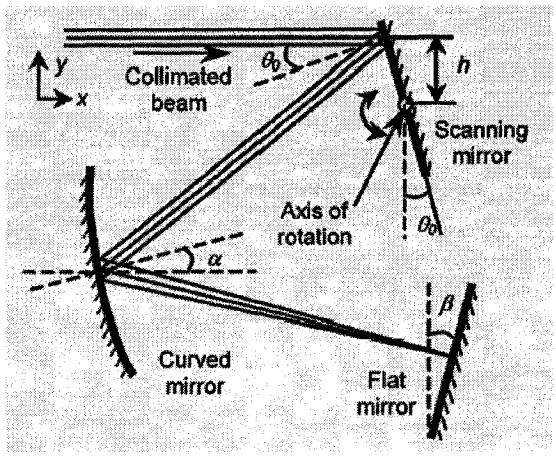

Figure 1-12. Schematic of the rapid-scanning all-reflective optical delay line [11].

The scanning mirror is placed close to the focal plane of the curved mirror, and the collimated bean is incident upon the scanning mirror with an offset relative to the axis of rotation. As the first mirror scans over a finite angular range, the center rays of the scanning focused beans will be

quasi-parallel to one another. The second flat mirror retroreflects the quasi-parallel beans back to the system [11].

1.4.3 SODLs based on optical fiber stretchers

A delay line based on stretching the fiber coiled around a cylindrical piezoelectric transducer has been reported. With many fiber windings, the small expansion of the PZT actuator can create several millimeters of delay [13].

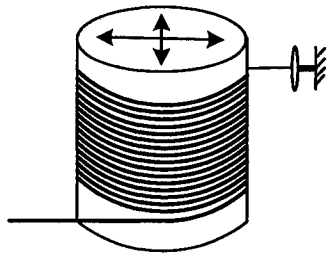

Figure 1-13. Schematic of an ODL base on optical fiber stretching [13].

1.4.4 SODLs based on group delay generation using Fourier domain optical pulse shaping technology

Fourier-domain delay lines, developed from femtosecond pulse-shaping technology, have been demonstrated to also be capable of shaping the temporal properties of broadband incoherent light. They achieve a linear group delay by applying a linear phase to the pulse in the Fourier plane of the pulse shaper. In this way, a variation in the reflection angle of a mirror placed in the Fourier plane can be used to produce a time delay. The advantage of this design is that group and phase delay can be tuned independently [7].

1.4.4.1 Tilting mirror

This SODL is based on a mirror acting as a spatial phase filter, imposing a linear phase ramp in the frequency domain [7]

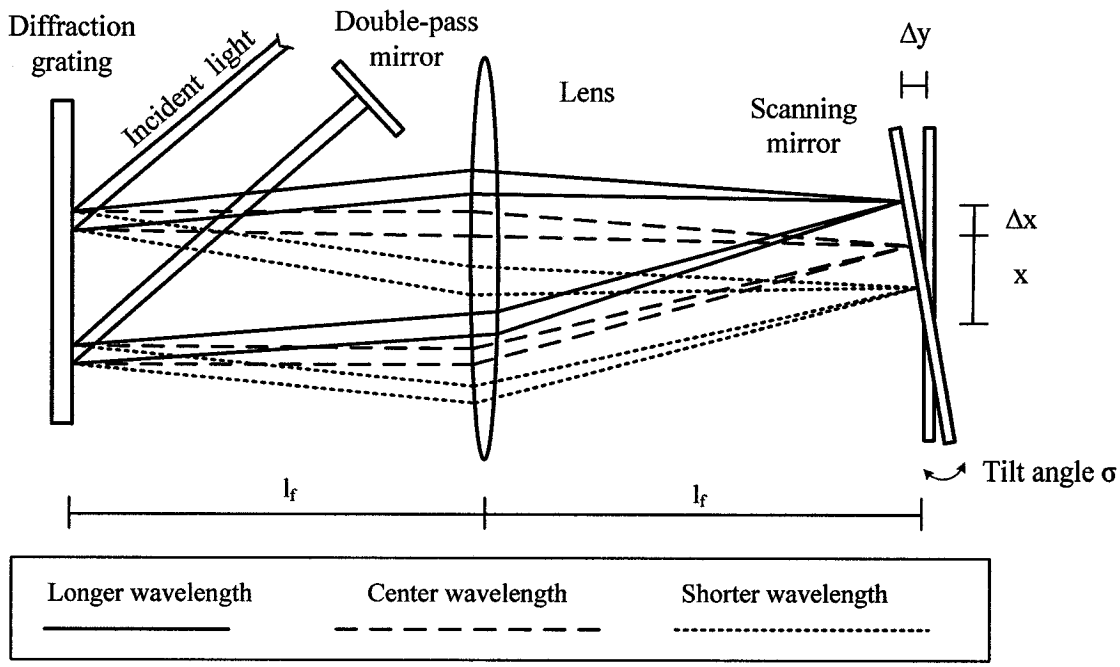

Figure 1-14. Schematic of a Fourier domain optical delay line with a tilting mirror (view from above) [7].

The incident, collimated broadband light is diffracted from the grating and spectrally dispersed. The lens collimates the dispersed spectrum while focusing it to a line on the scanning mirror. The scanning mirror imposes a linear phase ramp on the spectrum and redirects the light back through the lens. The lens re-collimates the beam and reconverts the spectrum onto the grating. The beam then diffracts in a reverse manner from the grating and propagates towards the double-pass mirror collinear with the incident beam collimated and undispersed. The double-pass mirror returns the light back through an identical path [7].

1.4.4.2 Polygonal scanner

A polygonal scanner is a Fourier-domain delay line that is scalable to higher speed without limiting the mirror size due to the fact that the delay element is a rotating polygon mirror array [8].

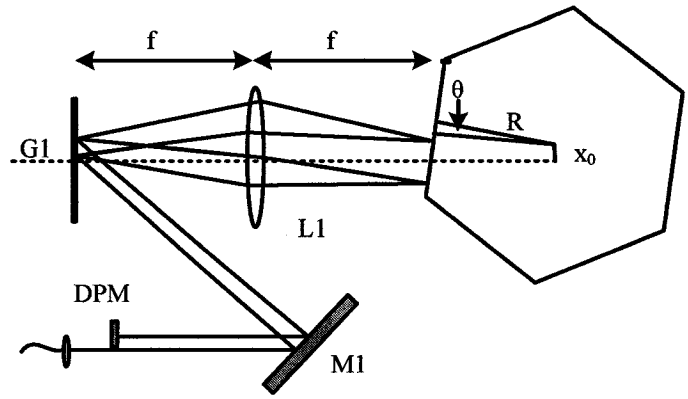

Figure 1-15. Schematic illustration of a Fourier-domain delay line with a polygonal mirror array [8].

The basic design of a double-pass Fourier domain delay line with a polygonal mirror array as the delay element is shown in Figure 1-15. R is the inner radius of the mirror array, θ is the scan angle, f is the focal length of the achromatic lens, and x_0 is the offset of the pivot point of the mirror array from the optical axis. The advantage of a double-pass design is that the amount of group delay is doubled and the transverse displacement over the scan angle can be counteracted. Light from the fiber interferometer is collimated and directed toward a grating where it is reflected at normal incidence to minimize Group Velocity Dispersion (GVD). The angularly dispersed light is imaged onto the surface of a polygon mirror by an achromatic lens .The light is reflected from the scanning mirror where it travels back through the system to the double pass mirror and it is retroreflected [8].

1.4.5 SODLs based on acousto-optical modulators

A fast ultrafine tunable delay line at 1550 nm by use of acousto-optic shaping has also been reported [19].

In acousto-optic ultrafast pulse shaping, a large-aperture acousto-optic modulator (AOM) is placed in the central Fourier plane of a zero-dispersion line, which consist of a pair of gratings and lenses in a 4-F configuration. Light incident upon the first grating spreads out in space and is collimated by the first lens. In the central Fourier plane the light is dispersed along the transverse

spatial axis so that the AOM can impose both amplitude and phase modulation upon it. The second pair of gratings and lens then re-collects the modulated spectrum. According to the displacement theorem of Fourier transformation, such a modulated pulse is related to the input phase by a simple time delay. In an acousto-optic pulse-shaping setup this spectral linear phase modulation can be achieved by imposition of a temporal linear phase modulation upon the driving voltage to the AOM, which corresponds to a simple shift of the center radiofrequency [19].

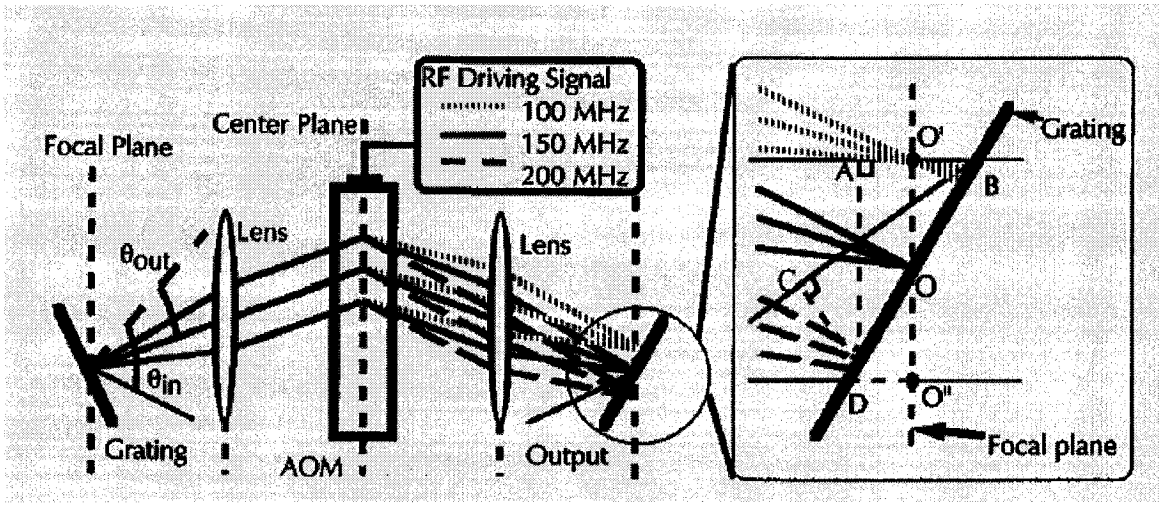

Figure 1-16. Schematic of a SODL based on the Fourier pulse shaper configuration. In this case the configuration is unfolded and acousto-optic modulator is used to generate a scanning phase ramp [19].

If the grating is chosen specifically so that θ_{out} for the center wavelength is zero (normal to the grating plane), the broadening factor will be zero and the delayed pulses will keep their original pulse width to first order. This ultrafine optical tunable delay could also be used as an ultrafine time-domain multiplexer [19]. This SODL was not developed for OCT, but in principle the technology could be used for these types of applications [13, 19, 20].

1.4.6 Comparison of the different categories of SODLs

In the below sections, some of the advantages and drawbacks of each configuration are summarized.

1. **Linear translation of retroreflective elements**

1) Linear translator mounted retroreflector (translating mirror, PZT stack)

Advantages:

- Very simple.
- Very flexible, able to operate with a wide range of scan lengths and scan velocities.
- The optical power loss (caused by imperfect reflectivity of the retroreflector and imperfect coupling of light) will be minimal using this type of SODL.
- Have no significant polarization or dispersion effects [13].

Disadvantages:

- Some degree of nonlinearity in its motion.
- Repetition rate of only 30 Hz when a millimeter scanning is required, which is too slow for many applications [13].

2) Multipass translating retroreflector

Advantages:

- Scans of 2-3 mm at repetition rates greater than 100 scans/ s.
- If high quality mirrors are used, optical power loss can be very small.
- High duty cycle (85%) [13].

Disadvantages:

- Because of non-normal incidence, optical power losses have polarization dependence.
- Power consumption required for generating acceleration increases dramatically with frequency and scanning range [13].

3) Galvanometer-Mounted Retroreflector

Advantages:

- Scan several millimeters.
- High duty cycle. [13]

Disadvantages:

- . Scanning velocities limited by inertia to be approximately 30 cm/s with repetition rates of 100 Hz and scan range of 3 mm, which is too slow for many applications [13].

4) Multi- pass cavity delay line

Advantages:

- 2 KHz repetition rate, scan speed of 6 m/s.
- Supports broad spectral bandwidths or short pulse durations.
- The cavities are easy to construct and long paths can be achieved in a small volume.
- Accumulates differential delays with each pass, enabling millimeter delays to be generated with tens of micrometer displacements.
- Sensitivity predicted > 100 dB.
- Low cost [10].

Disadvantages:

- Group delay nonlinearity (<10%).
- Parasitic modulation (10%) because of beam fluctuations during actuation of the scanner [10].

2. SODLs that vary optical pathlength by rotational methods

1) Rotating cube

Advantages:

- Scan velocity up to 95 m/s over a range of 120 mm and a repetition rate of up to 28 KHz, thus, an important motivation for this type of SODL is speed [13].

Disadvantages:

- Rather low duty cycle if the linear part of the scan is considered.

- The scan is not linear: the group delay is not a linear function of the rotation angle.
- Pathlength dependent dispersion.
- The scan range is not adjustable, it is fixed for a given cube size [13].

2) Scanning mirror

Advantages:

- Higher speed than SODLs based on linear translation of retroreflective elements
- No significant scan-dependent polarization or dispersion variation [13]

Disadvantages:

- Pathlength difference limited by the need to keep the scanning mirror within the depth of focus of the lens and by the size of the lens and mirrors [13]

3) Rotary mirror array

Advantages:

- Repetition scan rate of 2400 Hz over a 2 mm range
- Frequencies of interference signals are depth independent and limited to a relatively narrow band, which is highly desirable for optical Doppler tomography.
- A narrow band filter can be used to achieve a high signal-to-noise ratio.
- Duty cycle > 94%.
- Much more energy is saved than in vibrating devices. Mechanical vibrations and noises can also be reduced.
- Excellent linearity.
- Not suffer from group velocity dispersion [17].

Disadvantages:

- Untested on in vivo samples.
- Mirror array is highly customized [17].

4) KHz SODL with a set of identical wedge prisms

Advantage:

- Scanning amplitude ~3.5 mm and independent from scanning rate or rotation speed of the wheel.
- Free from angular dispersion.
- 99% scanning linearity.
- 95% duty cycle.
- Constructed with simple optics and driven by simple electronics [18].

Disadvantages:

- A small deviation from perfect linearity is expected as a result of the circular motion of the wheel [18].

5) All-reflection delay line with scanning mirror

Advantages:

- High repetition rates (4.1 kHz).
- High duty cycle (89%).
- Nondispersive.
- Low cost.

Disadvantage

- . Some nonlinearity in the delay line.

3. Fiber stretchers

Advantages:

- High repetition rates (1200Hz).
- Several millimeters of delay.
- High duty cycle (75%).

- Optical power loss equivalent to linear translation SODLs.
- Fits very well into the fiber optic technology [13].

Disadvantages:

- Temperature changes.
- Dynamic birefringence effects.
- Hysteresis effects.
- Polarization-mode dispersion.
- . Necessity of a high-voltage source for piezoelectric transducer driving [13].

4. SODLs that are based on group delay generation using Fourier domain optical pulse shaping technology

1) Tilting mirror

Advantages:

- High repetition rates (4 kHz).
- Several millimeters of delay.
- Group delay and phase delay can be adjusted independently [7].

Disadvantages:

- . Some nonlinearity in the phase delay and group delay.
- high order group-delay dispersion as well as the dispersion caused by optical component misalignment.
- High power loss caused by the grating [7].

2) Polygonal scanner

Advantages:

- Scalable to higher scan speed without limiting the mirror size.
- Linear in group delay (98.6%) over 2mm.

- GVD is expected to be negligible over this scan range.
- SNR of 80 dB.
- Group delay and phase delay can be adjusted independently [8].

Disadvantages:

- Some nonlinearity in the phase delay because of the geometry of the polygon, which causes chirp in the modulation signal.
- Low duty cycle.
- High power loss caused by the grating [8].

5. SODLs based on acousto-optical modulators.

Advantages:

- Can be generated ultrafine optical delays with a resolution smaller than 10-18s, a tuning range of >10 ps, and an update rate of microseconds.
- No moving parts needed.
- Can be used as an ultrafine time-domain multiplexer.
- Could be used in a feedback circuit to compensate actively for mechanical or thermal fluctuations [19].

Disadvantages:

- Optical power loss due to poor diffraction efficiency.
- Incompatibility with very broad optical bandwidths [19].

This section has reviewed the field of scanning optical delay lines (SODLs), emphasizing on devices that have been applied in OCT imaging. The delay lines have been classified in five categories. Advantages and disadvantages of each of them have been listed.

Chapter 2 Proposed Optical Delay Line and Theoretical Analysis

In this section, a novel multiple-pass cavity optical delay line is proposed and the theoretical analysis is given. Some parameters, which are crucial to the proposed delay line, are analyzed in detail in Section 2.2. The principle of optical components and parameters selection is given in Section 2.3.

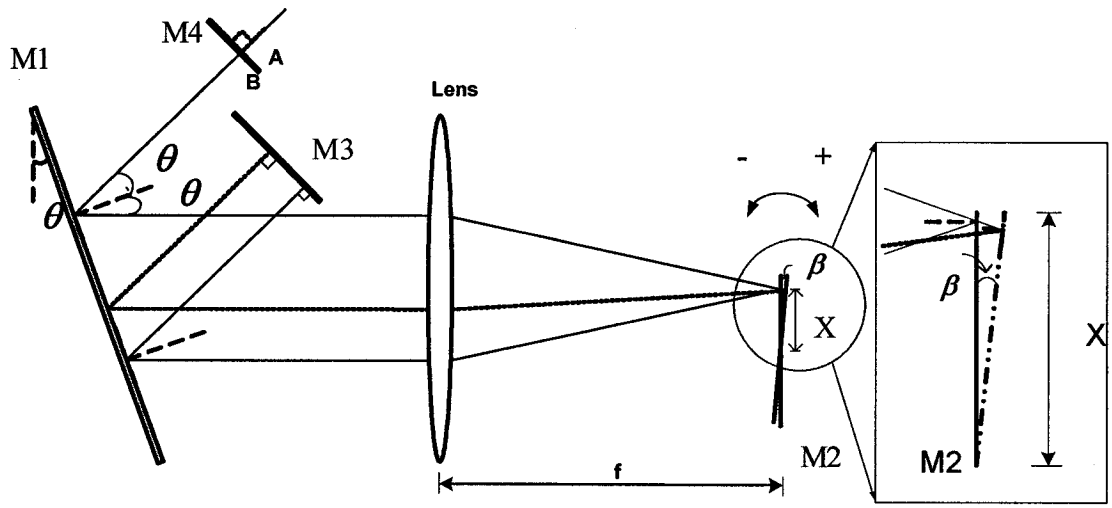

Figure 2-1. Schematic of the multiple-pass scanning optical delay line proposed. Dashed and solid lines represent two instances of ray paths.

2.1 Proposed optical delay line and theoretical analysis

The proposed delay line, which is schematically illustrated in Figure 2-1, can be classified as ODLs that vary optical pathlength by rotational methods. The proposed optical delay line consists of one achromatic lens, four mirrors and one resonant scanner. Suppose that the main axis of the delay line is the axis of the lens. Mirror M1 is tilted at an angle θ with respect to the focal plane of the lens. Mirror M2, the size of which is 6 mm x 5 mm driven by a resonant scanner, is located at another focal plane of the lens. The neutral position of M2 corresponds to the focal plane of the

lens. The incident collimated broadband light, whose incident angle is 2θ with respect to the main axis, first perpendicularly passes through mirror M4 whose reflectivities of A and B sides both are 0.5; then it is reflected by mirror M1 to the normal direction of the achromatic lens; the light is focused by the lens then hits the scanning mirror M2 at the focal point of the lens; the light, which is reflected by M2 back to the lens, goes through the lens and then travels at the normal direction of the lens; after the light hits mirror M1, it is reflected to the fold-pass mirror M3, which is tilted at the same angle as M4 is; since the light perpendicularly hits the M4, it is reflected back at the same path; when the light which is retro-reflected back at the same path through the whole delay line reaches mirror M4, half of the light energy passes through mirror M4 and couples back to optical fiber, and half of the light energy goes back to the delay line and passes through the delay line again due to M4 B-side 0.5 reflectivity. The route, which starts from mirror M4 and passes through all the components then ends at mirror M4, can be referred to as a single loop. Eventually, a chain of delayed signals will be generated from the optical delay line and coupled back to the optical fiber. The energy of the individual output delayed signal is given by:

$$E_n = E_0(1-R_{M4})R_{M4}^n \qquad \text{Eq. 2-1}$$

where E_0 is energy of the input signal, R_{M4} is the reflectivity of B side of mirror M4, n is the times of the same signal hitting mirror M4 from the inside of the delay line. The spacing between two consecutive output delayed signals is the length of the optical length of the delay line. The optical insertion loss of optical components is ignored.

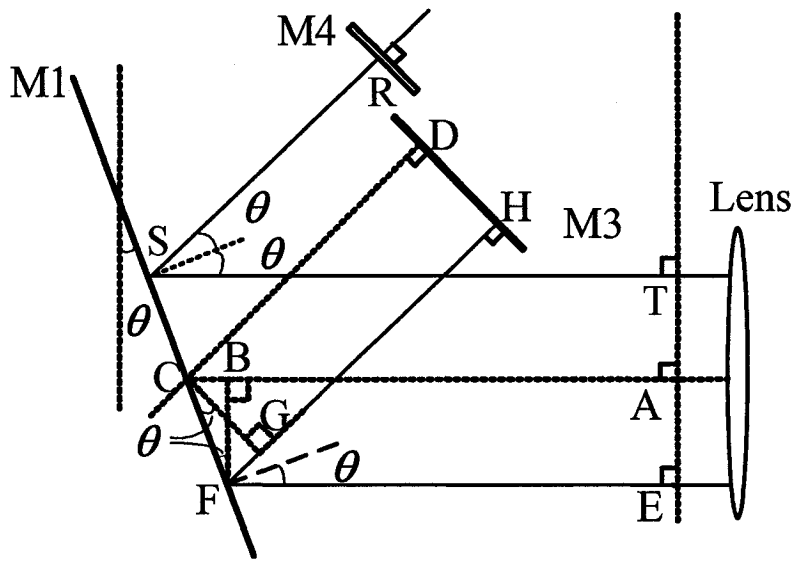

Figure 2-2. Left side of the optical delay line as shown in Figure 2-1.

Figure 2-2 shows the left part of Figure 2-1. In Figure 2-2, the path RST is the common path for all the rays. If we assume that lines AC and EF represent two arbitrary ray paths, it can be easily found that the path lengths of BC and FG are the same. Therefore, the path of ABCD = EFGH is obtained. This means that mirrors M1, M3 and M4 will not cause any optical path difference. Consequently, the only path difference will be raised from the scanning mirror M2. The scanning mirror M2 is tilting continuously during scanning. Each position of mirror M2 corresponds to a different delay. If the scanning angle is varied with time, the path difference (delay or advance) with time, with respect to the neutral position of the scanning mirror, is given by

$$l(t) = 4n\beta(t)X \qquad \text{Eq. 2-2}$$

where $\beta(t)$ is the tilt angle of mirror M2 with time as a variable, X is the pivot offset of mirror M2, factor of 4 takes into account the fact that the light passes through distance $\beta(t)X$ four times in a single loop, and n is the times of the desired delayed signal reaching mirror M4 from the inside of the delay line. Therefore the maximum path delay or advance of the whole delay line can be written as

$$l_{\max} = 2 \times 4n\beta_{\max} X = 4n\beta_{pp} X \quad \text{Eq. 2-3}$$

where β_{max} is the maximum single-side scanning angle, and β_{pp} is the peak-to-peak scanning angle ($\beta_{pp} = 2\beta_{\max}$). Eq. 2-3 shows that, for the given $l_{\max}$, if selected n is bigger than 1, a small value of X can be used. This means that a small-size scanning mirror can be used to generate a bigger path delay. Therefore, a high repetition rate of the delay line can be achieved by using a high speed resonant scanner to drive a small size scanning mirror. However the power of output delayed signals will be reduced if n is increased. For n=0, 1, and 2, the power of delayed signals is reduced by 3, 6, and 9 dB, respectively, if mirror M4 has 50% reflectivity at B-side. By considering the both output power and scanning speed, we choose the second output delayed signal as the desired delayed reference signal, i.e. n=2 chosen. If a resonant scanner is used to drive mirror M2, the scanning angle with time is given by:

$$\beta(t) = \frac{1}{2}\beta_{pp} \sin(2\pi f_{sc} t) \quad \text{Eq. 2-4}$$

where f_{sc} is the scanning repetition frequency. Therefore the path difference (delay or advance) of this proposed delay line is given by

$$l(t) = 8\beta(t)X = 4\beta_{pp} \sin(2\pi f_{sc} t)X \quad \text{Eq. 2-5}$$

The central frequency of the interference signal or interferogram (carrier frequency of the interferogram), which is determined by phase velocity, can be written as:

$$f_0(t) = \frac{1}{\lambda_0}\frac{\partial l}{\partial t} = \frac{8\pi f_{sc}\beta_{pp} X}{\lambda_0}\cos(2\pi f_{sc} t) \quad \text{Eq. 2-6}$$

where λ_0 is the central wavelength of the optical source. Eq. 2-5 and Eq. 2-6 show that optical path difference generated by the delay line and central frequencies of the interferogram vary sinusoidally with time, which is inevitable by using high-speed optical scanner.

The advantages and some drawbacks of the proposed delay line are summarized as follows:

Advantages:

- Supports broadband light source.
- High scanning repetition rate. This delay line is suitable for the OCT system which generates the high resolution and large dimension images at video rate.
- Simple.
- Low cost. All the components used in the delay line are inexpensive.
- Low effect of the group delay dispersion. The group delay dispersion, which is caused by aberration of the lens and misalignment of components, is greatly reduced. since all the frequency components travel together at any time.
- This delay line is flexible in changing the scan depth. The scan depth can be changed by changing the pivot of scanner mirror M2, the peak-to-peak scanning angle of M2, and the value of n.
- By choosing the high order delayed signal (n is bigger than 2) as reference signal, a higher speed resonant scanner can be used. Therefore, the scanning repetition rate can be increased.

Disadvantages:

- Nonlinearity. The path delay and carrier frequency of the interferogram vary sinusoidally with time are the major disadvantages of this delay line. However, this nonlinearity can be compensated by computer software.
- Power loss. The desired reference signal only carries a small part of energy of input signal. The power loss will increased with increasing the value of n.

2.2 Crucial noise component and crucial window

In the SODL of an OCT, each scanner scanning angle should only generate one delayed signal as a reference signal to interfere with signals returned from sample arm. At any given scanning angle, any signal, which is coupled back to interferometer from the delay line, other than desired delayed reference signal is noise. It is seen from Figure 2-1 that mirror M4 is used to form an optical cavity because B-side of mirror M4 has reflectivity. Such a cavity will increase optical delay time with a small pivot offset and a small scanning angle, and therefore a high speed scanning mirror can be used. However, due to this multiple-pass cavity, interference noise is introduced. Suppose that the optical signal source consists of a chain of short pulses with a repetition rate f_s, and time period $T_s = 1/f_s$. L_d, which varies with the scanning angle of mirror M2, is the delay line's single pass optical length which equals the optical path length of the loop, which starts from mirror M4 passes through all the components and goes back to M4. L_{d0} is the delay line's single pass neutral optical length, with respect to the neutral position of the scanning mirror. Hence L_d varies with time and the range of L_d is from $L_{d0} - l_{\max}/2n$ to $L_{d0} + l_{\max}/2n$. Due to the multiple-pass cavity, for each input signal or pulse a chain of infinite delayed signals are generated in principle. The delayed signals are referred to 0^{th}, 1^{st}, 2^{nd}, and 3^{rd}, ... order signals determined by times of the signal hitting M4 from the inside of the delay line. The time interval of the adjacent two delayed signals in the chain is given by $T_d = L_d/c$, where c is the velocity of the light. T_d also varies with time and T_{d0} corresponds to L_{d0}. Therefore for a given scanning angle, except the desired reference delay signal generated by current input signal, some other orders delayed signals generated by current and previous input signals are also coupled back from delay line into the interferometer. These signals are interference noise components. The sample signals returned from sample arm may interfere with some of these noise components. Based on the OCT principle we know that signals returned from sample arm and signals returned from

reference arm can interfere only if their time delays are matched. The time delays of sample signals vary from $2l_s/c$ to $2l_s/c+2\Delta l_{s,\max}/c$, where l_s is the optical length of sample arm and $\Delta l_{s,\max}$ is the light maximum penetration depth. This range can be referred as a crucial window and the width of the crucial window is denoted as T_w. Hence, the only noise components from the reference arm (or non 2nd-order delayed signals) whose time delays fall into a crucial window can cause false interference signals. These noise components are referred as crucial noise components which must be very small. To better understand these concepts, we consider delayed signals generated by the N^{th} -2, N^{th} -1, N^{th} and N^{th} +1 input signals, which are shown in Figure 2-3. Figure 2-3 (a) shows four input signals and corresponding reflected signal trains generated by the delay line, respectively. Figure 2-3 (b) shows the consecutive output signals of the delay line for the above four input signals. The time interval of the adjacent same order delayed signals is $T_s+\Delta t$, where T_s is the input signal repetition time and Δt is the small time delay due to the small angle change of scanning mirror M2. The best way to reduce those crucial noise components is to interleave the output delayed signals generated by adjacent input signals. The interleaving interval is determined by the ratio of the input signal repetition time T_s and time interval T_d. If T_d is compared with T_s, we can have $T_d \approx T_{d0}$. Suppose that

$$T_s/T_d = x_1 + x_2 \qquad \text{Eq. 2-7}$$

where x_1 is the integer and x_2 is the decimal fraction. Clearly x_1 is the times that signal hits mirror M4 from inside of delay line within T_s. To find the conditions that noise components will fall into crucial window and become crucial noise components, positive integer sets of (k_1, k_2) have to be found, where k_1 and k_2 must satisfy the condition of:

$$-T_w/2 < k_1 \cdot T_d - k_2 \cdot T_s < T_w/2 \qquad \text{Eq. 2-8}$$

Suppose that our considered crucial window is the N^{th} crucial window, a set of (k_1, k_2) means that one delayed output signal (noise component) generated by the N^{th} - k_2 input signal will fall into

current N^{th} crucial window. The ratio of the crucial noise component power and desired reference signal power is given by

$$r_{ns} = R_{M4}^{k_1} \approx R_{M4}^{k_2(T_s/T_d)} \approx R_{M4}^{k_2(x_1+x_2)} \quad \text{Eq. 2-9}$$

It is seen from Eq. 2-9 that there are three ways to reduce this noise impact. A first choice is to let the minimum k_2 as large as possible by carefully selecting the ratio of T_s/T_{d0}. Secondly, x_1 can be increased by reducing T_{d0}. A third choice is to reduce R_{M4}, the reflectivity of B side of mirror M4. Our simulation shows that the crucial noise components should be reduced to 2^{-37} times in power lower than the desired delayed signal (See section 3.3). Moreover, Eq. (1) shows that the focal length of the lens has no contribution to the optical path delay generated by the delay line. In our proposed delay line, a shorter focal length lens can be used so that a compact delay line can be obtained. On the other hand, a shorter focal length of the lens will result in a smaller T_{d0}. Thus, the crucial noise components are reduced due to increased integer x_1. In addition, because diffraction grating is not used in our proposed delay line, dispersion effect is significantly reduced.

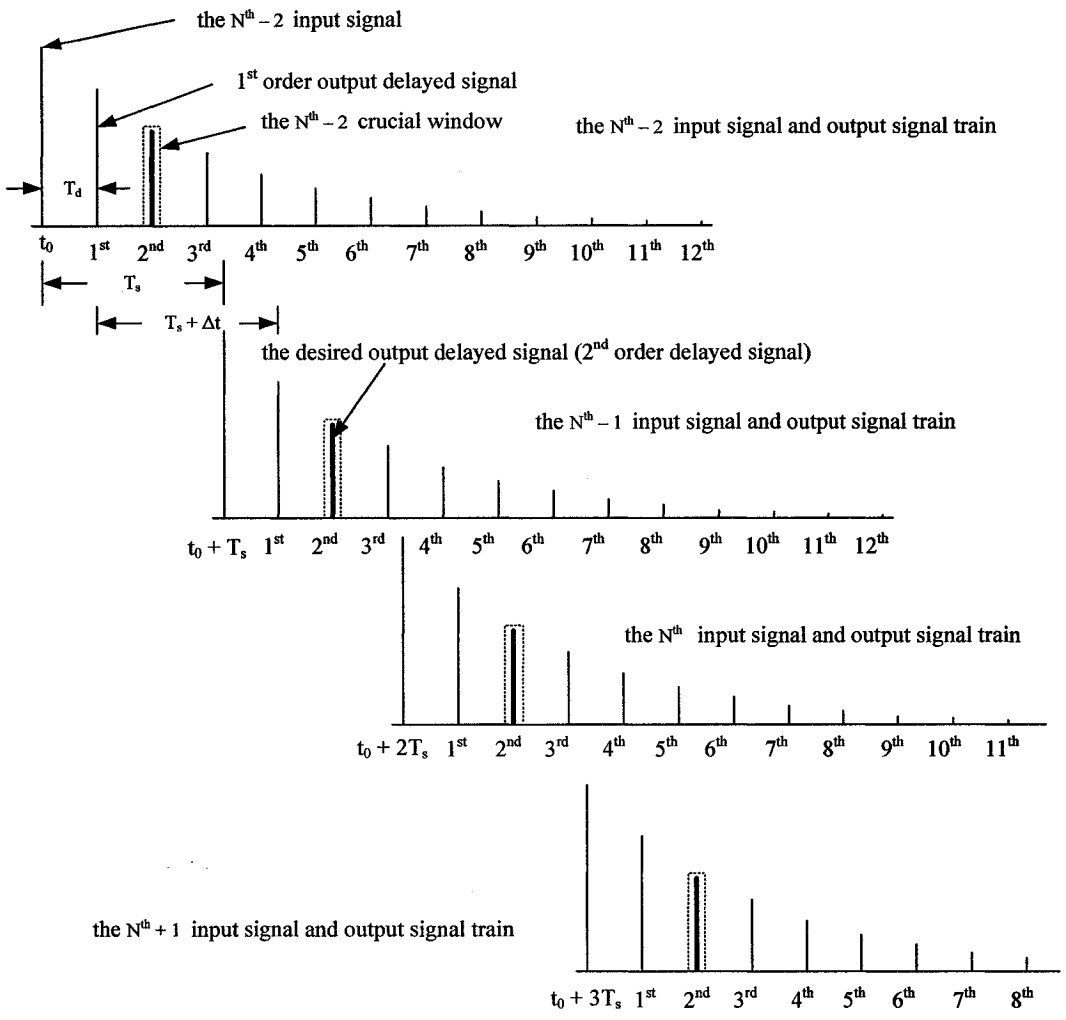

(a)

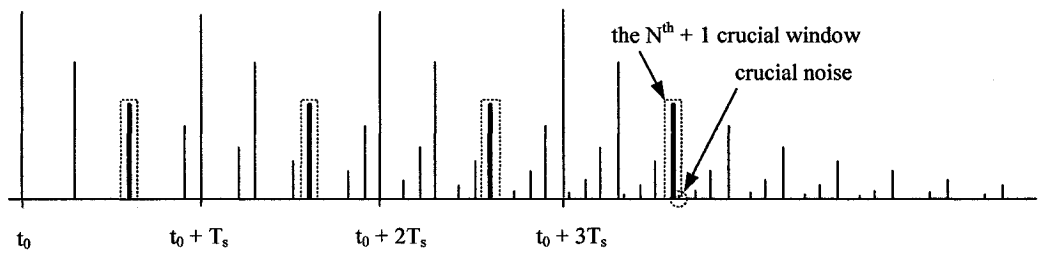

(b)

Figure 2-3. Output delayed multiple-pass signals generated by the delay line for (a) four input signals with time interval T_s (dashed lines) and the corresponding reflected signal trains (solid lines), respectively, and (b) consecutive output signals of the delay line. The crucial windows are indicated by dashed boxes and crucial noise is indicated in (b).

2.3 Principle of optical components and parameters selection

The aim of this section is to present the principle of selection of all optical components and parameters in the proposed delay line. The components and parameters used in this work also given at this section. Suppose that the maximum path delay l_{max} = 3 mm is required. The incident angle of the incident collimated broadband source light is 2θ with respect to the main axis of delay line.

1) Lens

In order to reduce the impact of aberration of lens, several rules should be obeyed in this delay line. First, an achromatic lens is preferred. An achromatic lens, which is shown in Figure 2-4, consists of a positive low-index crown glass lens element cemented to a negative high-index flint glass lens element. The elements are chosen so as to cancel chromatic aberration at two well separated wavelengths; usually in the blue and red region of the spectrum. Focal length is constant at those two wavelengths and focal length shifts are virtually eliminated across the visible wavelengths. The lens is computer designed to effectively minimize spherical aberration and coma aberration when operating at infinite conjugate ratio. Unlike singlet lenses, this results in a constant focal length independent of aperture and far better off-axis performance [23]. Second, a large diameter lens is preferred. Third, a lens with short focal length is preferred, since such a lens will help both to build up a compact delay line and to reduce the crucial noise components. Last, it is preferred to arrange light passing through the lens at the central part of the lens.

The main parameters of lens which is used in this delay line are (see 3.2.1)

Effective Focal length: f = 30 mm

Diameter: Dia = 25 mm

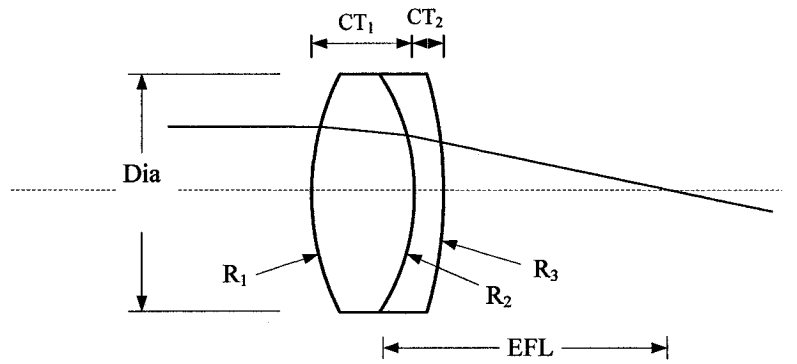

Figure 2-4. Schematic of an achromatic lens [23]

2) Optical scanner:

The scanning frequency of optical scanner is preferred to be as high as possible. However, the size of mirror, which will be driven by the optical scanner, limits the scanning frequency.

One of most commonly used optical scanner is SC-30 resonant optical scanner. The SC-30 type scanners are small size, long life, beam steering components which combine precision, accuracy, and excellent repeatability with high speed to generate, follow and control optical patterns. A scanner of this type operates at ONE FIXED FREQUENCY from the range of 200Hz to 16 kHz. While frequency is fixed, scan amplitude can be modulated. Scan rating can be doubled by scanning in both directions [22]. The main parameters of SC-30 are given in the Table 2-1

Table 2-1 Reference parameters of optical scanner SC-30 [22]

Frequency (Hz)	Scan angle (peak-to-peak) (degree)	Mirror size (mm)
200-750	30°	25x25 to 10x10
750-4000	20°	10x10 to 8x9
4000-6000	16°	8x9 to 7x8
6000-8000	12°	7x8 to 5x6
8000-10000	12°	5x6 to 4x5
10000-16000	6°	4x5 to 3x4
16000	5°	3x4

A 8 kHz resonant scanner is selected in this delay line. Therefore a repetition rate 16 kHz is achieved, if we record the both forward and backward strokes.

3) Mirror M2

As it shown in Table 2-1, in order to use a high speed resonant scanner, a small size mirror should be used. If a 8 kHz resonant scanner is used, then the maximum size of the mirror is 5×6 mm. Since the pivot of the mirror M2 is in the middle of M2, the pivot offset of M2 should be less than half of the width of mirror. After taking into account the impact of mirror tilting, the pivot offset is preferred to be as large as possible in order to maximum the usage of the mirror.

The main parameters of mirror M2 in this work are (see 3.2.1)

Size: 5×6 mm

Pivot offset: 2.4 mm

Position: at the right focal plane of lens

Required peak-to-peak scanning angle:

$$\beta_{pp} = \frac{l_{\max}}{8X} = 3\times10^{-3}/(8\times2.4\times10^{-3}) = 0.15625(rads) = 8.953^{\circ}$$

4) Mirror M1

Mirror M1 should be tilted at an angle θ with respect to the focal plane of lens L1. The distance between the center of M1 and the center of lens L1 can be selected arbitrarily. In this work, mirror M1 is located at the left focal point of L1.

In order to calculate of the minimum size of M1, the schematic of the delay line is re-drawn in Figure 2-5. In Figure 2-5, ray path 1 represents the common path for all the rays, ray paths 2, 3, and 4 represent three ray instances with respect to M2's tilt angles of $-\beta_{\max}$, 0 and $\beta_{\max}$, respectively. As mentioned above, the ray path 1 should close to axis as much as possible to reduce the impact of the aberration of the lens. However ray path 1 should be above ray path 2, otherwise, some signals will couple back to optic fiber through mirror M4 without hitting mirror M3. The minimum size of mirror M1, which is the length of OR, is:

$$l_{M1,\min} = h/\cos\theta \qquad \text{Eq. 2-10}$$

Since ray 1 should very close to ray 2, we can have

$$h \approx l_{PS} = h_1 + h_2 \qquad \text{Eq. 2-11}$$

where l_{PS} is the length of line PS and

$$h_1 \approx f \times tg(\beta_{\max}) \times 2 \qquad \text{Eq. 2-12}$$

$$h_2 \approx f \times tg(\beta_{\max} + 2\beta_{\max}) - f \times tg(\beta_{\max}) \qquad \text{Eq. 2-13}$$

where f is the focal length of lens L1. Therefore,

$$\begin{aligned} l_{M1,\min} &= h/\cos\theta \\ &\approx (f \times tg(\beta_{\max} + 2\beta_{\max}) + f \times tg(\beta_{\max}))/\cos\theta \\ &\approx 11.5\ mm \end{aligned}$$

The minimum size of mirror M1 is ~ 11.5 mm. In this work, a mirror with size 30x30 mm is used as M1 (see 3.2.1).

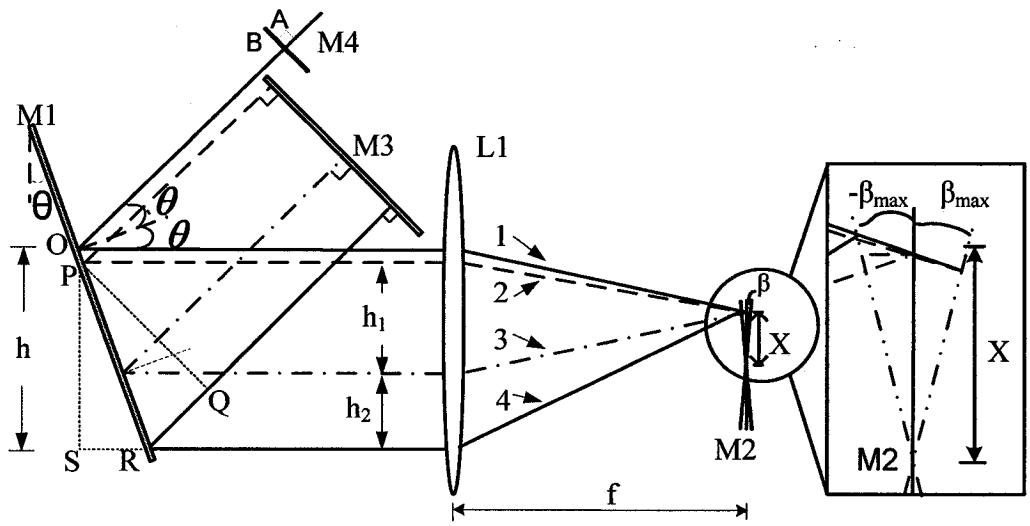

Figure 2-5. Schematic of the multiple-pass scanning optical delay line. Ray path 1 represents the common path for all the rays, ray paths 2, 3, and 4 represent three ray instances with respect to M2's tilt angles of $-\beta_{\max}$, 0 and $\beta_{\max}$, respectively.

The main parameter of mirror M1 in this delay line are:

Size: 30 x 30 mm

Position: center of mirror is located at left focal point of L1

Angle of tilting: θ with respect to the focal plane of lens

5) Mirror M3

Mirror M3 should be tilted at an angle $\pi/2-2\theta$ with respect to the axis of delay line. The minimum width of mirror M3, denoted as $l_{M3,\min}$, equals l_{PQ}, which is the length of PQ.

$$l_{M3,\min} = l_{PQ} = l_{PS} = h_1 + h_2 \qquad \text{Eq. 2-14}$$

$$\Rightarrow \quad l_{M3,\min} = 9.83\ mm$$

In this work, a mirror with size of 15x15 mm is used as fold-pass mirror M3.The distance between the center of M3 and the center of M1 can be adjusted according to the required T_{d0}.

The main parameter of mirror M3 in this delay line are:

Size: 15x15 mm

Angle of tilting: $\pi/2-2\theta$ with respect to the axis of delay line

6) Mirror M4

Mirror M4 should be tilted at an angle $\pi/2-2\theta$ with respect to the axis of delay line. The size of mirror M4 is not a big issue, as long as it can accommodate the collimated input light spot which is very small. The distance between the center of M4 and the center of M1 can be adjusted according to the required T_{d0}.The reflectivity of A side of M4 is preferred to be 0 in order to minimize the power loss. In order to obtain the maximum output power of the desired signal, from Eq. 2-1, the reflectivity of B side of M4 R_{M4} should satisfy:

$$\frac{dE_n}{dR_{M4}} = 0 \qquad \text{Eq. 2-15}$$

$$\Rightarrow \quad E_0 \times \left[nR_{M4}^{n-1} - (n+1)R_{M4}^{n} \right] = 0 \qquad \text{Eq. 2-16}$$

$$\Rightarrow \quad R_{M4} = \frac{n}{n+1} \qquad \text{Eq. 2-17}$$

However a large R_{M4} may increase the power of crucial noise components. Therefore in this work, $R_{M4} = 0.5$ is chosen when parameter n = 2 is selected.

The main parameters of mirror M4 in this work are:

Size:	10x10 mm
Angle of tilting:	$\pi/2-2\theta$ with respect to the axis of delay line
Reflectivity of B side:	$R_{M4} = 0.5$
Reflectivity of A side:	1 - $R_{M4} = 0.5$

The theory of the proposed delay has been analyzed in this chapter. In next chapter, computer simulations have been done to verify the proposed delay line.

Chapter 3 Verification by Computer Simulation

The proposed optical delay line is verified by computer simulations. All the computer simulation modules in this work are coded and run in Matlab and Simulink platform.

3.1 OCT system components and parameters used to verify the delay line

In order to verify the proposed delay line, an OCT module has been built. The components and parameters used to construct the OCT module are:

1) Signal light source

A Gaussian pulse signals generator is used as signal source. The Gaussian pulse signal has a central wavelength of λ_0=1550 nm with a full width at half-maximum (FWHM) spectral width of 210 nm. The source is normalized to unit power. The pulse is repeated with a frequency of f_s=256 MHz which corresponds to a time interval of T_s=3.9 ns.

2) Interferometer

A 50-50 coupler is used as the interferometer.

3) Detector

A basic photodiode is used as the detector.

4) Components in the sample arm

To verify this proposed delay line, we assume that there is a mirror, whose reflectivity is 100%, on a translation mounted in the OCT sample arm. For a simple analysis, we set the zero delay point at the M2 tilt angle of zero (neutral position). However, the zero delay point can be set at any M2 tilt angle by adjusting the OCT sample arm length. It should be noticed that the path delay of a sample signal is 2 times the path difference between the sample mirror and the neutral position of the sample mirror.

3.2 Basic verification of the proposed delay line

The purpose of the first simulation, referred as Simulation One, is to verify the basic properties of the proposed delay line. Suppose that the maximum path delay $\Delta l_{\max} = 3$ mm is required.

3.2.1 Components and parameters in the reference arm (delay line)

Components and parameters used in the reference arm (the proposed delay line) are listed as follows

1) The incident angle of light

The incident angle of light $\theta = 30°$ is chosen.

2) The delay line's single pass neutral optical length

$L_{d0} = 348$ mm is chosen. Therefore the $T_{d0} = L_{d0} / c = 1.161$ ns is obtained.

3) The width of crucial window

Since the maximum scan length $\Delta l_{\max} = 3$ mm is required, the required maximum penetration depth is 1.5 mm in the air and the width of crucial window T_w=10 ps is obtained.

4) n, the times of desired delayed reference signal reaching mirror M4 from inside of delay line:

The 2nd order delayed signal is used as the desired reference signal. Thus, the parameter n=2 is chosen.

5) Scanner:

A resonant scanner SC-30, whose scanning frequency $f_{sc} = 8$ kHz, is used. The scanning angle, which varies with respect to time, is given by [22]:

$$\beta(t) = \frac{1}{2}\beta_{pp} \sin(2\pi f_{sc} t)$$

At this scanning frequency, the scanner can drive a 5 x 6 mm mirror and the maximum peak-to-peak scanning angle of the scanner is 12°.

6) Lens

An achromatic lens, the schematic is shown in Figure 2-4, is used in this simulation. Main parameters of the lens used in the simulations are [23]:

Effective Focal Length (EFL): f = 30.00 mm

Diameter: Dia = 25.00 mm

Center Thickness 1: CT_1 = 11.04 mm

Center Thickness 2: CT_2 = 11.04 mm

Radius of Curvature (surface 1): R_1 = 21.17

Radius of Curvature (surface 2): R_2 = 16.08

Radius of Curvature (surface 3): R_2 = 118.66

Glass Type: (BaF10) – (FD10)

Index of refraction of glasses: (1.670) – (1.728)

7) Mirror M1

A mirror with a reflectivity of 100% is used as mirror M1. Other parameters of M1 used in the simulations are:

Size: 30 x 30 mm

Position: the center of mirror is located at left focal point of the lens

Angle of tilting: 30° with respect to the focal plane of lens

8) Mirror M2

A mirror with a reflectivity of 100% is used as mirror M2 and is driven by the scanner SC-30. Other parameters of M2 used in the simulations are:

Size: 5×6 mm

Position: at the right focal plane of lens L1.

Pivot offset: 2.4 mm

Maximum required peak-to-peak scanning angle:

$$\beta_{pp} = \frac{l_{\max}}{8X}$$
$$= 3\times10^{-3}/(8\times2.4\times10^{-3})$$
$$= 0.15625(rads)$$
$$= 8.953°$$

This required peak-to-peak scanning angle is less than SC-30's maximum peak-to-peak scanning angle, which is 12°.

9) Mirror M3

A mirror with a reflectivity of 100% is used as mirror M3. Other parameters of M3 used in the simulations are:

Size: 15x15 mm

Position: the distance between the center of M3 and the center of M1 is 10.23 mm

Angle of tilting: 30° with respect to the axis of delay line

10) Mirror M4

A mirror with a reflectivity of one side (A side) 0 and a reflectivity of another side (B side) R_{M4} = 0.5 (since n =2 is chosen for this delay line as mentioned before) is used as mirror M4. Side A of mirror M4 is faced to the incident light. Other parameters of mirror M4 in this delay line are:

Size: 10x10 mm

Angle of tilting: 30° with respect to the axis of delay line

Position: the distance between the center of M4 and the center of M1 is 10.76 mm

3.2.2 Ray tracing result

Ray tracing results of the proposed delay line with different tilt angles of mirror M2 are shown in Figure 3-1, respectively. Figure 3-1 (a), (b) and (c) show that the output lights follow the same paths of the input lights when the tilt angles of mirror M2 are positive. Figure 3-1 (d) and (e)

show that the output lights are slightly walk off from the incident light when the tilt angles of mirror M2 are negative. The reasons of this walking off are: first, the light incident point of mirror M2 is not exactly at the focal point when mirror M2 is tilted; second, some points at which light passes through the lens are far off-axis points of the lens when the tilt angles of M2 are negative. Therefore, to reduce this walking off, mirror M2 is preferred to have a large diameter. So that all (or most) of the points, at which light passes through the lens in the proposed delay line, are near-axis points of the lens.

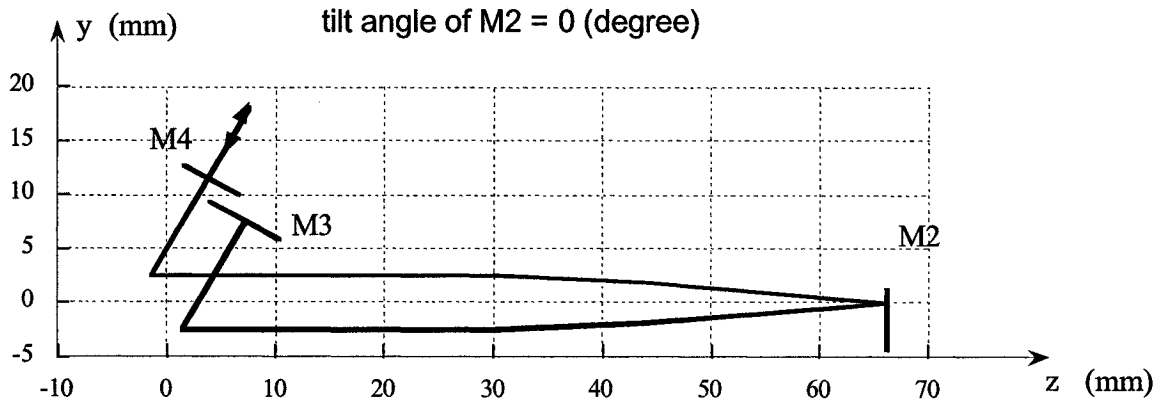

(a)

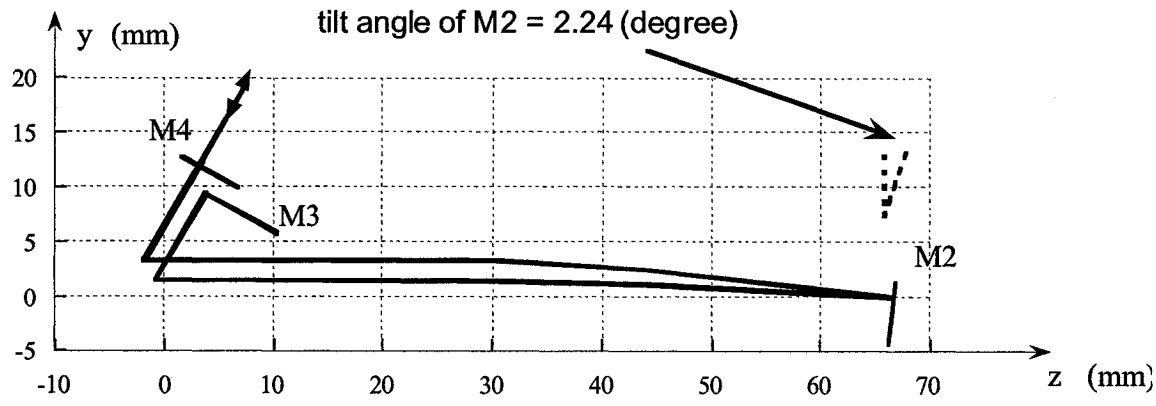

(b)

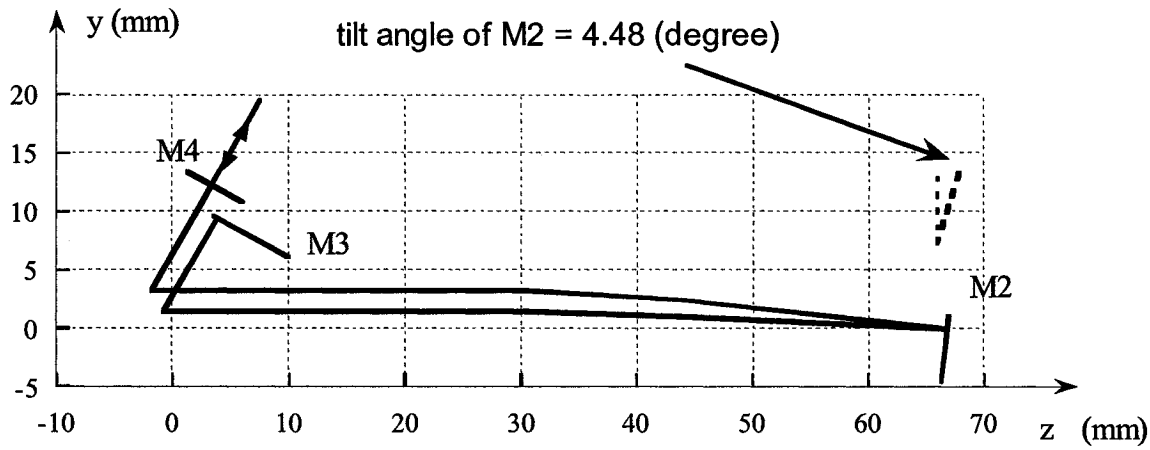
y (mm)
tilt angle of M2 = 4.48 (degree)
20
15
10
5
0
-5
M4
M3
M2
-10
0
10
20
30
40
50
60
70
z (mm)

(c)

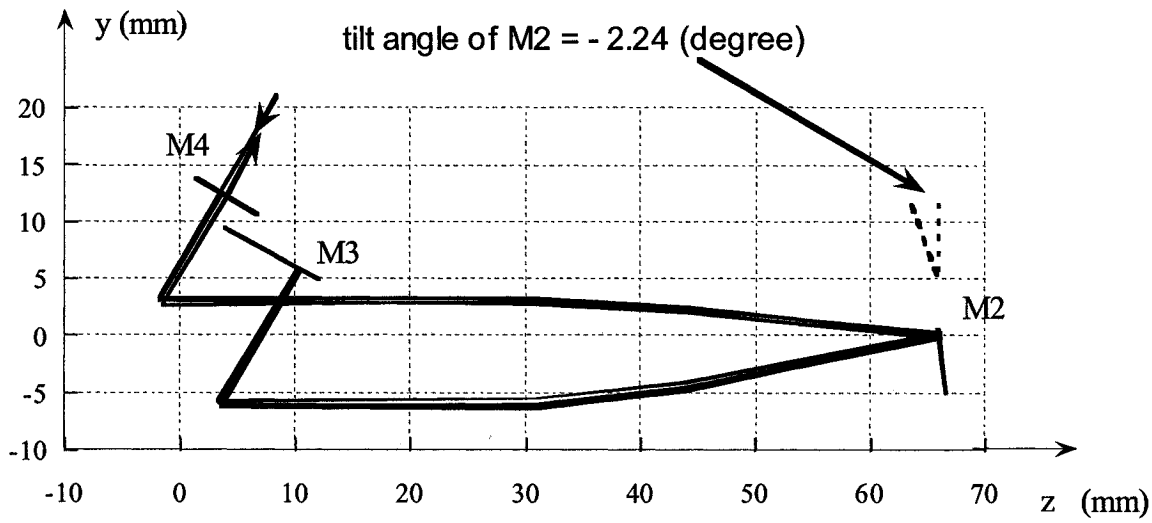
y (mm)
tilt angle of M2 = - 2.24 (degree)
20
15
10
5
0
-5
-10
M4
M3
M2
-10
0
10
20
30
40
50
60
70
z (mm)

(d)

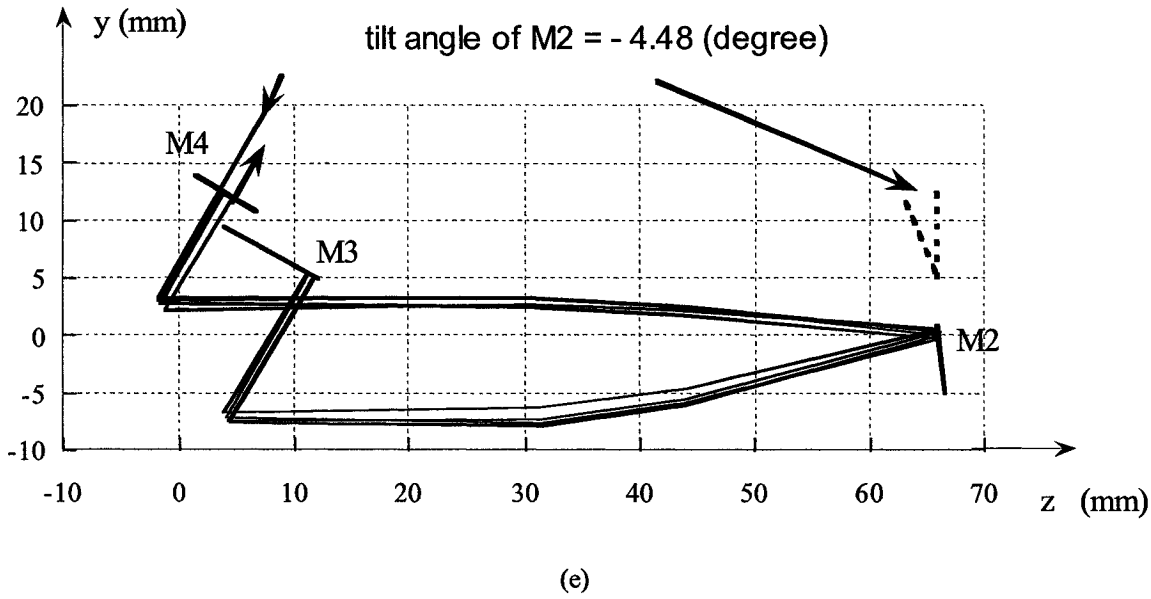

(e)

Figure 3-1. Ray tracing results of Simulation One.

3.2.3 Properties of the proposed delay line

Since the scanner's scanning frequency f_{sc} is 8 kHz, the time period of a forward stroke or a backward stroke of scanning is:

$$\frac{1}{2}\frac{1}{f_{sc}} = 62.5 \ \mu s$$

Figure 3-2 shows a detected OCT signal during one forward stroke of scanning. This electrical OCT signal is obtained by the delayed reference signals, which are returned from the proposed delay line, beating with a 50 μm delayed signal which is returned from the OCT sample arm. In order to show the detail of this OCT signal, a re-scaled signal is shown in Figure 3-3. Figure 3-3 clearly shows that the OCT signal has a Gaussian envelope and is modulated by a carrier. The peak of the OCT signal is occurred at time 31.915 μs. To find out the carrier frequency of this OCT signal, the frequency spectrum of this OCT signal is shown in Figure 3-4. From Figure 3-4, it can be found that the center frequency (carrier frequency) of the OCT signal is ~48.265 MHz and the signal's FWHM is ~4.90 MHz.

Two other OCT signals are obtained and shown in Figure 3-5 and Figure 3-6. The corresponding spectrums of these OCT signals are shown in Figure 3-7 and Figure 3-8. These OCT signals are obtained by the signals returned from delay line interfering with a 350 μm delayed sample signal and a −200 μm delayed sample signal, respectively. The peaks of the OCT signals are occurred at 35.99 μs and 28.57 μs respectively. The carrier frequencies of the OCT signals are ~46.99 MHz and 47.05 MHz respectively. The FWHM of the OCT signals are ~4.90 MHz and 4.89 MHz respectively.

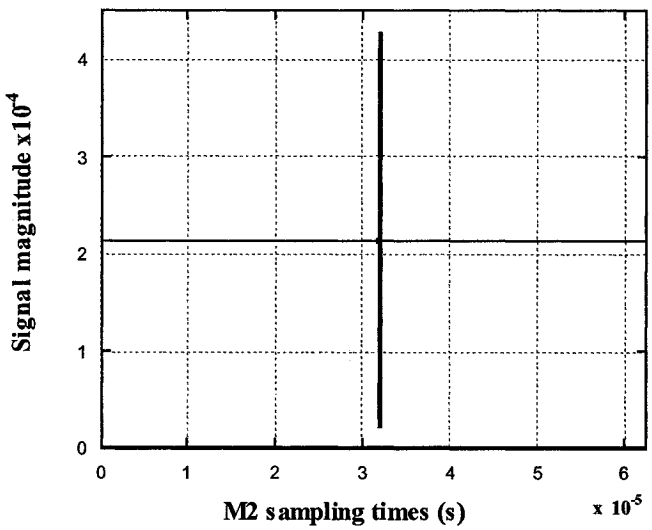

Figure 3-2. An OCT signal obtained by signals returned from the reference arm interfering with a 50 μm delayed signal returned from the sample arm

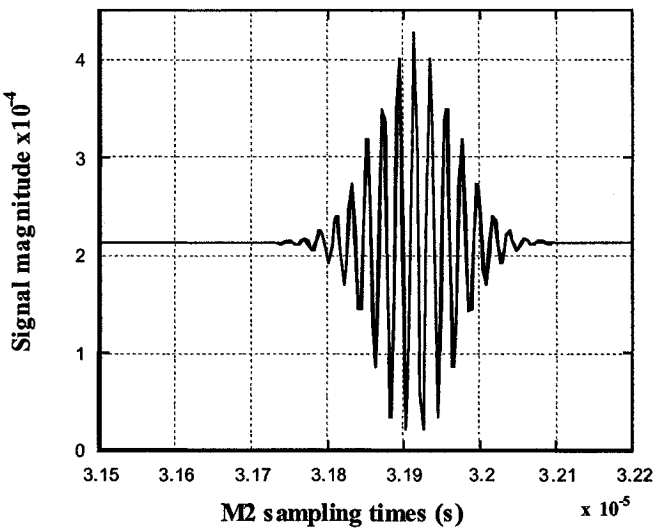

Figure 3-3. Re-scaled OCT signal which is shown in Figure 3-2

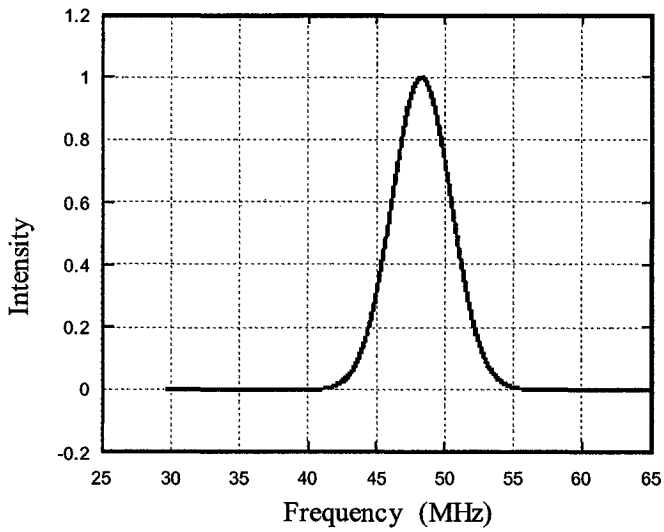

Figure 3-4. Frequency spectrum of the OCT signal shown in Figure 3-2.

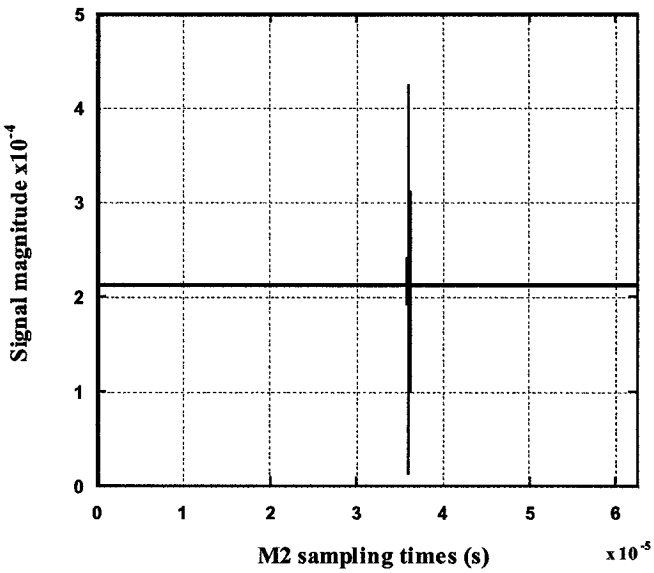

Figure 3-5. An OCT signal obtained by signals returned from the reference arm interfering with a 350 μm delayed signal returned from the sample arm

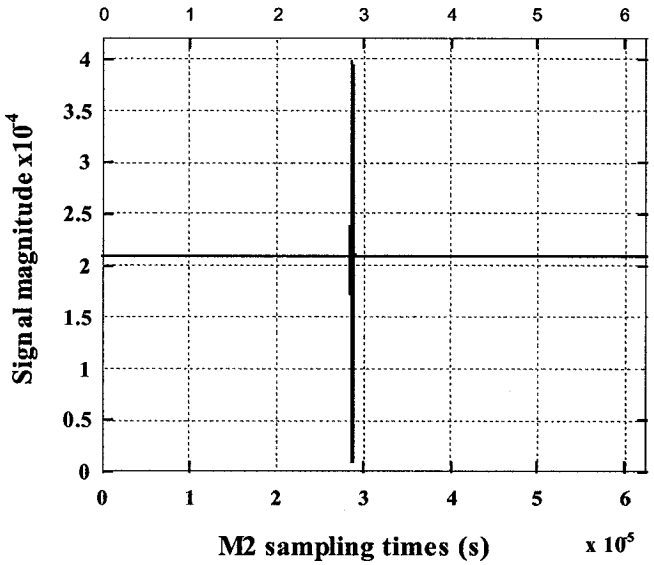

Figure 3-6. An OCT signal obtained by signals returned from the reference arm interfering with a -200 μm delayed signal returned from the sample arm

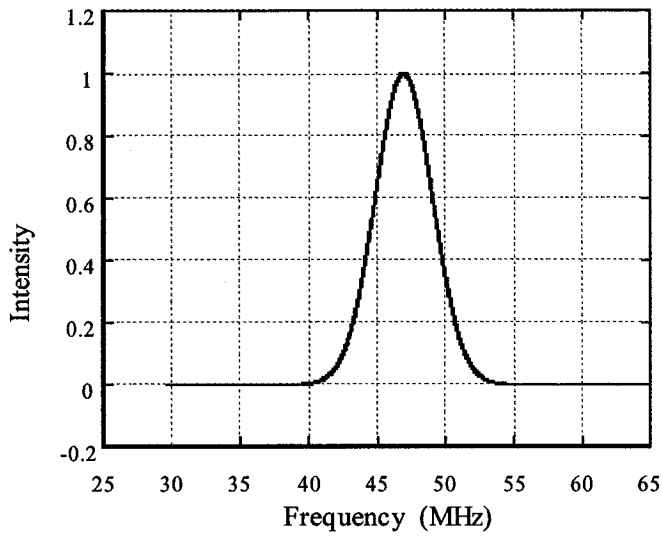

Figure 3-7. Frequency spectrum of the OCT signal shown in Figure 3-5

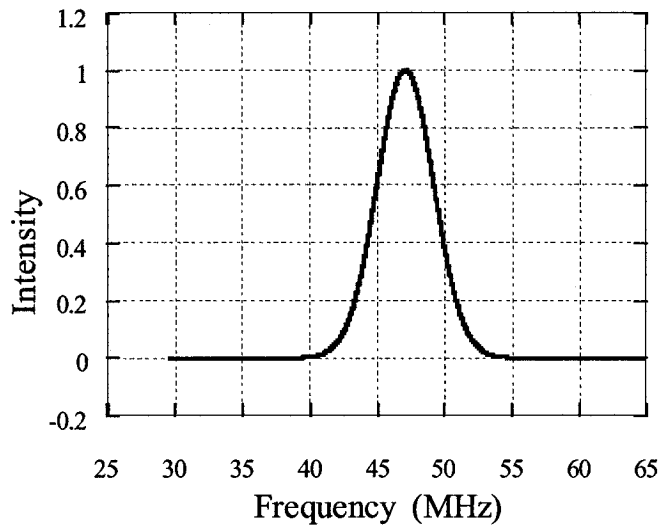

Figure 3-8. Frequency spectrum of the OCT signal shown in Figure 3-6

By comparing Figure 3-2, Figure 3-5 and Figure 3-6, it is shown that the time at which an OCT signal occurs corresponds to a path delay of a reference signal (or a sample signal). Thus, each tilt angle of mirror M2 corresponds to a different path delay. By adjusting the position of the sample mirror in the sample arm, we measure OCT signal occurring time, as shown in Figure 3-9, and measure the carrier frequencies of OCT signals, as shown in Figure 3-10.

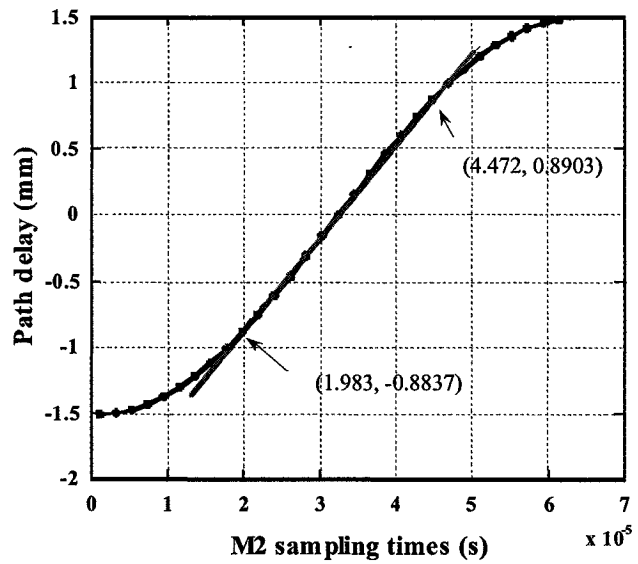

Figure 3-9. Path delay as function of OCT sampling time

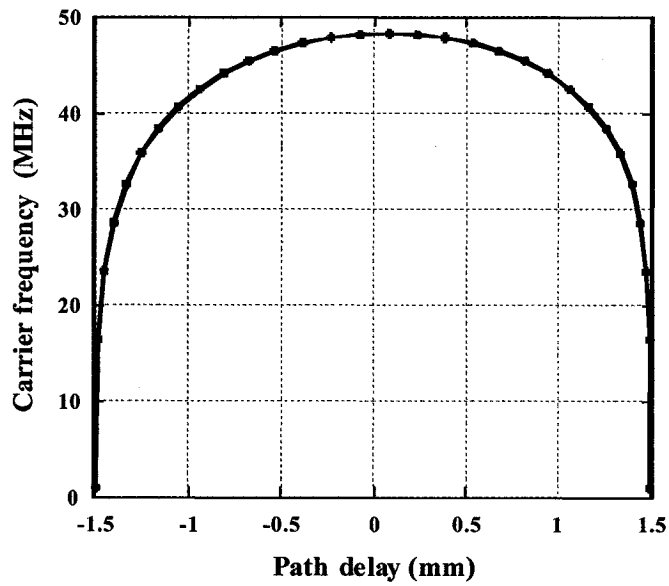

Figure 3-10. Carrier frequency of the interferogram as function of path delay

From Figure 3-9 and Figure 3-10, the following properties of the delay line can be obtained.

- The scanning repetition rate

A repetition rate 16 kHz is achieved since a 8 kHz optical scanner was used and both forward and backward strokes were recorded. This repetition rate can support 533 transverse lines per image at video rate (30 images per second).

- The total path delay

The total path delay is ~3 mm which is agreed with the requirement. From Figure 3-9, it can be found that the path delay generated by the delay line varies sinusoidally with time;

- The linear range of the path delay

The linear range of the path delay is ~2.3 mm. The straight line, as shown in Figure 3-9, is the best fit for the linear region.

The total path delay and the linear range of path delay can be increased by setting M2's peak-to-peak scanning angle of larger than 8.96°.

- The scanning velocity in the linear region

From Figure 3-9, the scanning velocity in the linear region of path delay can be calculated as $(0.8903 - -0.8837)\times10^{-3}/\,[(4.472 - 1.983)\times10^{-5}] \approx 71.3$ m/s.

- The duty circle

If only the linear region is considered and both forward and backward strokes are recorded, the duty circle is ~66%.

- The carrier frequency of OCT signals

The theoretical maximum carrier frequency of the OCT signal is

$$f_{0,\max} = \frac{8\pi f_{sc}\beta_{pp}X}{\lambda_0} = 48.56 \text{ MHz}$$

From Figure 3-10, it can be found that the carrier frequencies of the interferogram vary sinusoidally with time. The maximum carrier frequency of OCT signal is 48.4 MHz which quite match the theoretical calculation. If the linear path delay region is only considered, the carrier frequencies of OCT signals range from 38 MHz to 48.4 MHz. This carrier frequency variation will cause the detection bandwidth increased; therefore, the signal-to-noise ratio (SNR) of OCT signals will be degraded.

By moving the mirror in the sample arm during one forward stroke of scanning, multiple sample signals with different path delay can be simulated. When these sample signals interfere with the

signals returned form the delay line, detected signals are similar to the signals in real OCT system. Figure 3-11 shows OCT signals which are detected during one forward stroke. These OCT signals are obtained by the signals returned for the delay line interfering with sample signals with path delay of -1400 μm, -1200 μm, -1000 μm, -800 μm, -600 μm, -400 μm, -200 μm, 0 μm, 200 μm, 400 μm, 600 μm, 800 μm, 1000 μm, 1200 μm, and 1400 μm respectively.

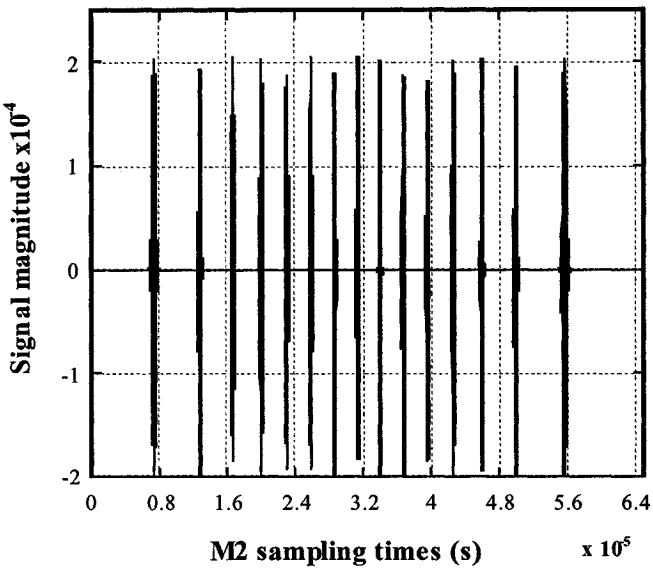

Figure 3-11. OCT signals obtained in one forward stroke of scanning.

3.3 Advanced verification of the proposed delay line

3.3.1 The impact of the crucial noise

Some other computer simulations are done to verify the impact of the crucial noise and the effect of the interleaving interval T_i.

- maximum tolerable ratio of the noise component and the desired reference signal in power

A simulation is done to find out the ratio of the maximum tolerable power of the noise component and the power of a desired reference signal. In this simulation, a crucial noise component is added to the delayed signals returned from delay line. The crucial noise component is 30 μm delayed

compared with the desired signal. The mixed signals interfere with a 350 μm delayed signal returned from the sample arm. By adjusting the power of the added crucial noise component, six figures of interferogram are obtained and shown in Figure 3-12, respectively. In Figure 3-12, P_s is the power of the desired signal and P_n is the power of the crucial noise component; the real OCT signals are generated by the desired delayed signals interfering with the sample signals; the false interference signals are generated by the crucial components interfering with the sample signals. Figure 3-12 (f) shows that the false interference signal is almost unrecognizable when $P_n / P_s < 10^{-11} \approx 2^{-37}$. This means that the dynamic range of OCT system is 110dB.

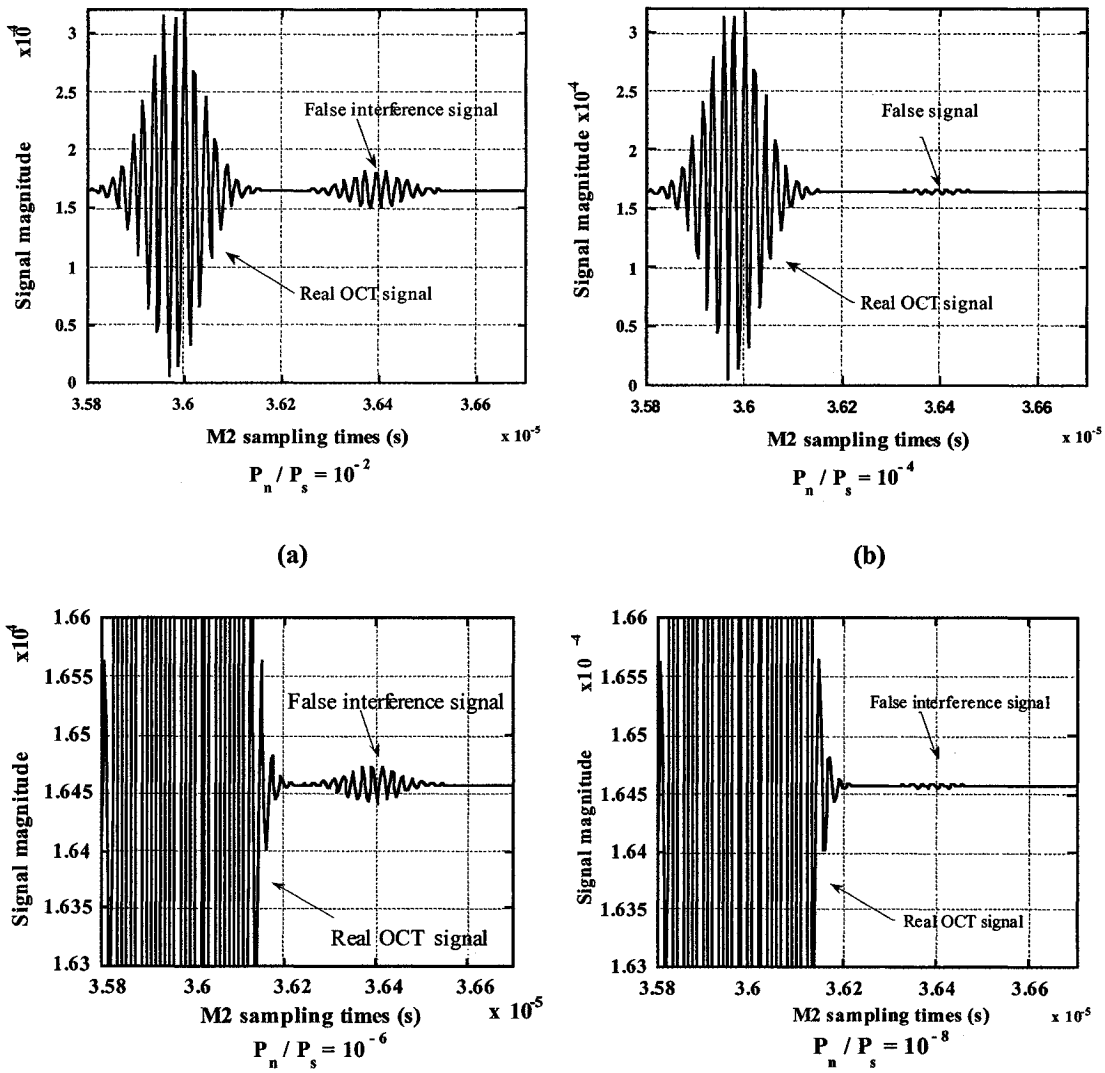

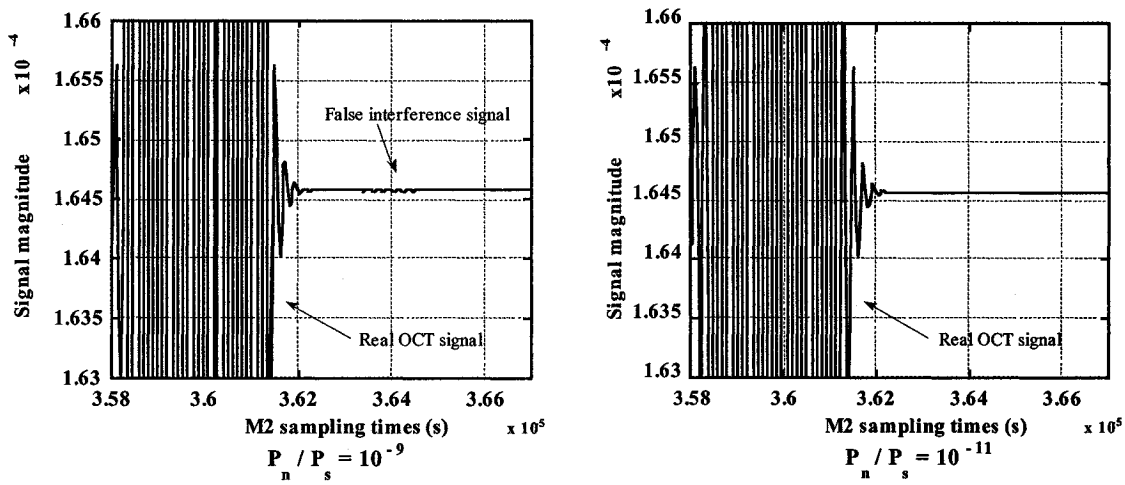

Figure 3-12. Impact of the power of the crucial noise components

3.3.2 The impact of the interleaving interval T_i

To achieve the ratio of $P_n / P_s < 10^{-11} \approx 2^{-37}$, all crucial noise components should be high orders delayed signals and orders of these crucial noise components are at least 39 (37 + n = 39). To control the orders of crucial noise components, we can control T_i by choosing T_{d0}.

Some simulations are done to verify the impact of T_i. In these simulations, all the components of the delay line except mirror M3 are at the same positions as those in the Simulation One. By adjusting the position of M3, different L_{d0} or T_{d0} can be obtained. Therefore the different interleaving interval T_i can be used to show the impact of the crucial noise. When T_{d0} = 1.116 ns (or $T_s / T_{d0} = 3.5$) is chosen and a 50 μm delayed signal is used as the sample signal, the detected OCT signal is shown in Figure 3-13 (a). Figure 3-13 (a) shows that, in addition to the desired OCT signal, the false interference signals are induced. These false interference signals are generated by the crucial noise components. In order to clearly show the false interference signals, we re-plot the false interference signals with a small scale as shown in Figure 3-13 (b).

To analysis the detail of crucial noise components, which generate the false interference signals shown in Figure 3-13, data of the signals returned from the delay line at time 31.915 μs

(corresponds to path delay 50 μm) are shown in Table 3-1. In Table 3-1, the centralized time delay T_{cd} is obtained by subtracting $2T_{d0}$ from the time delay of the signal components returned from the delay line. Therefore $T_{cd} = 0$ corresponds to the zero path delay point of the proposed delay line. As mentioned before, except the desired delayed signal all other signals are noise components. A noise component is a crucial noise component, if the centralized time delay of the noise component satisfies the condition:

$$-\frac{T_w}{2} < T_{cd} < \frac{T_w}{2} \qquad \text{Eq. 3-1}$$

where T_w is the width of the crucial window and equals 10 ps in this simulation. From Table 3-1, it can be found that the crucial noise components are the 9th, 16th, 23rd, 30th, 37th and 44th order delayed signals. The crucial noise components whose order are higher than 44 are not shown in the table, since their power are so small and can be neglected. The crucial noise components, whose order are less than 39, cause the false interference signals shown in Figure 3-13.

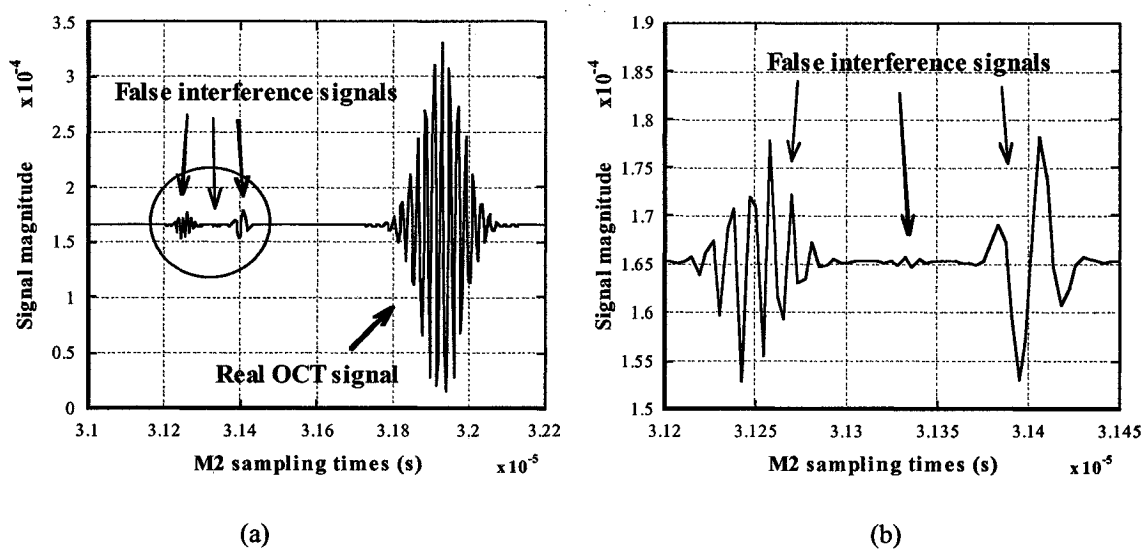

(a) (b)

Figure 3-13. (a) Real OCT signal and false interference signals caused by crucial noise components; and (b) re-scaled false interference signals which were shown in (a).

To demonstrate the impact of T_i, we also show the data, obtained in Simulation One in which T_{d0} = 1.16 ns (or $T_s / T_{d0} = 3.36$) is chosen, in Table 3-2. In Table 3-2 the data of signals returned

from the delay line are obtained at time 31.915 μs (corresponds to path delay 50 μm). From Table 3-2, it can be found that there is no crucial noise component whose order is less than 44. This means that the delay line is immune form the crucial noise component in Simulation One.

From all these simulation, it was shown that the selection of T_i is very important for this delay line. By carefully selecting the ratio of T_s and T_{d0}, the crucial noise components can be reduced to a significant low level (only very high-order delayed signals which are very weak may fall into the crucial window).

Table 3-1. Signals returned from the delay line at time 31.915 μs (corresponds to path delay 50 μm). T_{d0} = 1.116 ns (or $T_s / T_{d0} = 3.5$).

Relative signal number compared with the current signal	Times of signal reaching M2 from inside of delay line	Centralized time delay (ps)	comment
0	1	-1115.9881	
0	2	0.1666	Desired signal
0	3	1116.3214	
-1	5	-557.6172	
-1	6	558.5376	
-2	8	-1115.3995	
-2	9	0.7552	Crucial noise
-2	10	1116.9100	
-3	12	-557.0251	
-3	13	559.1296	
-4	15	-1114.8041	
-4	16	1.3507	Crucial noise
-4	17	1117.5054	
-5	19	-556.4263	
-5	20	559.7284	
-6	22	-1114.2018	
-6	23	1.9529	Crucial noise
-6	24	1118.1077	
-7	26	-555.8207	
-7	27	560.3341	
-8	29	-1113.5928	
-8	30	2.5620	Crucial noise
-8	31	1118.7167	
-9	33	-555.2082	
-9	34	560.9466	
-10	36	-1112.9769	
-10	37	3.1779	Crucial noise
-10	38	1119.3326	
-11	40	-554.5889	
-11	41	561.5659	
-12	43	-1112.3542	
-12	44	3.8006	Crucial noise
-12	45	1119.9553	

Table 3-2. Signals returned from the delay line at time 31.915 μs (corresponds to path delay 50 μm). T_{d0} = 1.16 ns (or $T_s / T_{d0} = 3.36$).

Relative signal number compared with the current signal	Times of signal reaching M2 from inside of delay line	Centralized time delay (ps)	comment
0	1	-1160.9582	
0	2	0.1666	Desired signal
0	3	1161.2915	
-1	5	-422.7069	
-1	6	738.4180	
-2	8	-845.5789	
-2	9	315.5460	
-2	10	1476.6708	
-3	11	-1268.4495	
-3	12	-107.3241	
-3	13	1053.8007	
-4	15	-530.1928	
-4	16	630.9321	
-5	18	-953.0599	
-5	19	208.0649	
-5	20	1369.1898	
-6	21	-1375.9257	
-6	22	-214.8003	
-6	23	946.3245	
-7	25	-637.6641	
-7	26	523.4608	
-8	28	-1060.5264	
-8	29	100.5985	
-8	30	1261.7233	
-9	31	-1483.3872	
-9	32	-322.2619	
-9	33	838.8630	
-10	35	-745.1208	
-10	36	416.0041	
-11	38	-1167.9782	
-11	39	-6.8529	
-11	40	1154.2720	
-12	42	-429.7083	
-12	43	731.4165	

3.3.3 The impact of other parameter

One simulation is done to verify the impact of the peak-to-peak scanning angle of the scanner. In this simulation, all the components are in the same place as those in Simulation One. We only change the peak-to-peak scanning angle of the scanner to the maximum peak-to-peak scanning angle 12° or 0.2094 rads.

According to the Eq. 2-3, the maximum path delay should be

$$\begin{aligned} l_{\max} &= 4n\beta_{pp}X \\ &= 4\times 2\times 0.2094\times 2.4 \\ &= 4.02\ mm \end{aligned}$$

One of simulation results, the path delay as function of OCT sampling time, is shown in Figure 3-14.

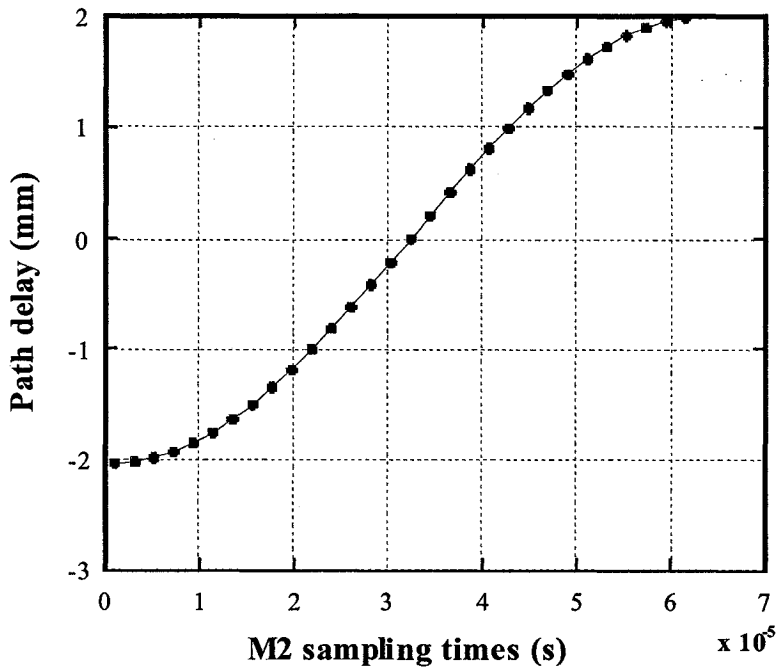

Figure 3-14.Path delay as function of OCT sampling time. The peak-to-peak scanning angle of the scanner is set to 12°.

From Figure 3-14, it can be found that repetition rate is 16 kHz; the total path delay is ~ 4 mm which quite agrees with the theory calculation; the linear range of the path delay is ~3.1 mm; the

scanning velocity in the linear region of path delay is ~95 m/s; the duty circle is ~ 66% if the only the linear region is considered and both forward and backward strokes are recorded.

Chapter 4 Conclusion and Future Works

4.1 Major contribution

In this work, a novel high speed optical delay line based on optical multiple-pass cavity is proposed and theoretical analysis of the proposed delay line is presented. The crucial parameters of the proposed delay line are analyzed and the principles of the optical components selection are given. Computer simulations are done to verify the proposed delay line. Computer simulation modules are coded and run in Matlab and Simulink platform.

The basic simulation shows that 16 kHz repetition rate can be achieved and this repetition rate can support 533 transverse pixels per image at video rate. The maximum path delay is ~3 mm, the scanning velocity is 71.3 m/s with a duty cycle of ~66%. The advanced simulations show that this delay line may suffer from interference noise due to the multiple-pass cavity. However, we showed that by carefully selecting the delay line parameters, the detected interferogram cannot be interfered by this noise.

The major advantages of the proposed delay line are high speed and broadband light source supporting. Therefore, the proposed delay line is especially suitable for the OCT that will generate the large dimension images at video rate with high resolution. Because the diffraction grating is not used in our proposed delay line, dispersion effect is significantly reduced. This is another advantage of the proposed delay line.

The maximum path delay and the scanning velocity can be increased by setting the scanner's peak-to-peak scanning angle of bigger than 8.96°. If a higher-order delayed signal is used for the reference signal, the repetition rate of up to 32 kHz can be realized by using a smaller scanning mirror driven by a high speed resonant driver.

4.2 Future works

In this work, some conditions are considered ideally in the computer simulations. The light source signal and photodetector are noise free. Dispersion caused by chromatic aberration of the lens is not considered in the simulations. All the mirrors are considered perfectly. Therefore more complex simulation modules should be constructed in the future to verify the proposed delay line. The most important future job is to test the delay line in a real OCT system.

References and links

1. D. Huang, E. Swanson, C. Lin, J. Schuman, W. Stinson, W. Chang, M. Hee, T. Flotte, K. Gregory, C. Puliafito, and J. Fujimoto, "Optical coherence tomography," Science **254**, 1178-1181 (1991).
2. W. Drexler, U. Morgner, F. Krtner, C. Pitris, S. Boppart, X. Li, E. Ippen, and J. Fujimoto, "In vivo ultrahigh-resolution optical coherence tomography," Opt. Lett. **24**, 1221-1223, (1999).
3. I. Hartl, X. D. Li, C. Chudoba, R. Ghanta, T. Ko, J. Fujimoto, J. Ranka, and R. Windeler, "Ultrahigh-resolution optical coherence tomography using continuum generation in an air silica microstructure optical fiber," Opt. Lett. **26**, 608-610, (2001).
4. Y. Wang, Y. Zhao, J. Nelson, Z. Chen, Robert and S. Windeler, "Ultrahigh-resolution optical coherence tomography by broadband continuum generation from a photonic crystal fiber," Opt. Lett. **28**, 182-184, (2003).
5. K. Kwong, D. Yankelevich, K. Chu, J. Heritage, and A. Dienes, "400-Hz mechanical scanning optical delay line," Opt. Lett. **18**, 558-560, (1993).
6. G. Tearney, B. Bouma, and J. Fujimoto, "High speed phase- and group-delay scanning with a grating-based phase control delay line," Opt. Lett. **22**, 1811-1813, (1997).
7. A. Rollins, M. Kulkarni, S. Yazdanfar, R. Ung-Arunyawee, and J. Izatt, "In vivo video rate optical coherence tomography," Opt. Express **3**, 219-229, (1998).
8. A. Oldenburg, J. Reynolds, D. Marks, S. Boppart, "Fast-Fourier-domain delay line for in vivo optical coherence tomography with a polygonal scanner," Appl. Opt. **42**, 4606-4611, (2003)
9. R. Windecker, M. Fleischer, B. Franze and H. Tiziani, "Two methods for fast coherence tomography and topometry," J. Mod. Optics, **44**, 967-977, (1997).

10. P. Hsiung, X. Li, C. Chudoba, I. Hartl, T. Ko, and J. Fujimoto, "High-speed path-length scanning with a multiple-pass cavity delay line," Appl. Opt. **42**, 640-648, (2003).

11. M. Liu, M. Cobb and X. Li, "Rapid scanning all-reflective optical delay line for real-time optical coherence tomography," Opt. Lett. **29**, 80-82, (2004).

12. E. Smith, A. Zvyagin, and D. Sampson, "Real-time dispersion compensation in scanning interferometry," Opt. Lett. **27**, 1998-2000, (2002).

13. B. Bouma and G. Tearney, Handbook of Optical Coherence Tomography, (Marcel Deckker, Now York, 2001).

14. E. A. Swanson, D. Huang, M. R. Hee, J. G. Fujimoto, C. P. Lin, and C. A. Puliafito, "High-speed optical coherence domain reflectometry," Opt. Lett. **17**, 151-153, (1992).

15. M. D. Kulkarni, T. G. van Leeuwen, S. Yazdanfar, and J. A. Izatt, "Velocity Estimation Accuracy and Frame Rate Limitations in Color Doppler Optical Coherence Tomography," Opt. Lett. **23**, 1057-1059, (1998).

16. J. A. Izatt, M. D. Kulkarni, H.-W. Wang, K. Kobayashi, and M. V. Sivak Jr., "Optical Coherence Tomography and Microscopy in Gastrointestinal Tissues," IEEE J. Sel. Top. Quant. Elect **2**, 1017-1028, (1996).

17. N. G Chen, and Q. hu, "Rotary mirror array for high-speed optical coherence Tomography," Opt. Lett. **27** (2002)

18. M. Lai,. "Kilohertz scanning optical delay line employing a prism array," Appl. Opt. **40**, 6334-6336, (2001)

19. W. Yang, D. Keusters, D .Goswami, and W. S. Warren, "Rapid ultrafine- tunable optical delay line at the 1.55 μm wavelength," Opt. Lett. **23**, 1843-1845, (1998)

20. J. V. Howe and C. Xu, "Ultrafast optical delay line by use of a time-prism pair," Opt. Lett. **30**, 99-101, (2005)

21. P. Hsiung, Y. Chen, T. H. Ko, and J G. Fujimoto, "Optical coherence tomography using a continuous-wave, high-power, Raman continuum light source," Opt. Expr. **12**, 5287-5295, (2004)
22. http://www.eopc.com/sc30.html
23. Commercial paper of Electro-Optical Products Corporation. http://www.edmundoptics.com
24. W. K. Niblack, J. O. Schenk, B. Liu, and M. E. Bbrezinski, "Dispersion in a grating-based optical delay line for optical coherence tomography," Opt. Expr. **42**, 4115-4118, (2003)
25. L. P. Sanz, "High speed optical delay line for optical coherence tomography," Thesis, Technical University of Denmark., 2004
26. A. V. Zvyagin, E. D. J. Smith, and D. D. Sampson, "Delay and dispersion characteristics of a frequency-domain optical delay line for scanning interferometry," J. Opt. Soc. Am., **20**, 333-341, (2003)
27. http://www.le.ac.uk/eg/fss1/DELAYS.DOC
28. http://www.sciences.univ-nantes.fr/physique/enseignement/english/theoric.html